Right-handed currents, finite neutrino mass, and mass mixings in K_{l3}^{+} decays

R. R. L. Sharma* and N. K. Sharma
Department of Physics, University of Rajasthan, Jaipur 302004, India
(Received 21 June 1985)

K_{l3}^{+} decays have been investigated with the inclusion of right-handed currents (RHC's), finite neutrino mass, and mass mixings. Predictions have been obtained for (i) pion energy spectrum, (ii) decay probability, (iii) π-l $(=e,\mu)$ angular correlations, (iv) π-l energy correlations, (v) lepton energy spectrum, (vi) π-ν_i $(i=e,\mu\tau)$ angular correlations, (vii) π-ν_i energy correlations, (viii) l-ν_i angular correlations, (ix) l-ν_i energy correlations, (x) the ratio $R=W(K_{\mu3}^{+})/W(K_{e3}^{+})$, and (xi) longitudinal lepton polarization. RHC contributions are transparent in almost all the parameters discussed, whereas finite-neutrino-mass contributions are substantial in (i)—(v), (x), and (xi). The distinction between RHC contributions and finite-neutrino-mass contributions is possible in (i)—(v), (x), and (xi). Mixing effects are in general negligible but could be perceptible in the parameters (ii), (v), (x), and (xi). It is shown that the currently known value of the ratio R can be understood with the inclusion of finite neutrino mass without or with RHC contribution. Lepton longitudinal polarizations (P_1), however, require the inclusion of the RHC contribution with or without the inclusion of finite $m(\nu_3)$. The range of neutrino mass $m(\nu_3)$ values obtained with the inclusion of the RHC factor lies between 14±8 and 44±5 MeV. The RHC-factor (F) limits are $F<0.26$ and $F<0.22$ for K_{e3}^{+} and $K_{\mu3}^{+}$ decay modes respectively, for vanishing $m(\nu_3)$.

I. INTRODUCTION

The $SU(2)_L\times U(1)$ electroweak theory[1] has met with astounding success in the discoveries at CERN of intermediate vector bosons[2] $W^{\pm},Z$, with characteristics exactly agreeing with the predictions of the theory. But there are a number of problems[3] which require extension of the theory to a higher-symmetry group that in a limit may reduce to this model. An appealing and minimal enlargement of this model is to base the theory on the gauge group[4–8] $SU(2)_L\times SU(2)_R\times U(1)$, which contains right-handed (RH) currents, besides the usual left-handed (LH) interactions. In an interesting version of this model,[8] spontaneous breakdown of symmetry is incorporated systematically, and the scale of parity restoration is related to the nonvanishing neutrino mass. Further, it may also provide an effective intermediate stage in breaking the symmetry of some of the grand unified theories[7] (GUT's).

These features have motivated a good deal of interest in these theories to make worthwhile theoretical and experimental efforts to see the effects predicted by these theories, as well as to constrain them. Notable among these have been those by (i) Beg, Budny, Mohapatra, and Sirlin,[9] who provide a comprehensive study of the experimental constraints on left-right-symmetry (LRS) theory from low-energy processes involving charged currents, (ii) Beall and Bander,[10] who find constraints on the mass scale of LRS theory from K_L-K_S mass differences, (iii) Oka,[11] who has attempted to solve the discrepancy between the Cabibbo-model predictions and the experiments on hyperon decay parameters, (iv) Keung and Senjanović,[12] who made definite predictions about the production of right-handed gauge boson (W_R), and (v) Masso's[13] work, which constrains the W_L-W_R mixing angle within the framework of a general Higgs sector, etc.

It is shown by Beall and Bander[10] that for equal LH and RH Kobayashi-Maskawa (KM) mixing angles and $g_L=g_R$, $g_{L,R}$ being left, right coupling constants, the experimental value of the K_L-K_S mass difference (Δm_K) imposes severe restriction on the right-handed-current (RHC) contribution, λ $(={m_L}^2/{m_R}^2)=3\times10^{-3}$, and as a consequence the contributions from RHC's in all low-energy leptonic and semileptonic decays are expected to be negligible. However, for unequal LH and RH angles, Herczeg and co-workers[14] have shown that the Δm_K value does not rule out large contributions from RHC's even in the low-energy leptonic and semileptonic processes; the possibility also includes muon number violation. This view has been further strengthened by the investigations of Oka,[11] who has resolved the discrepancy between the Cabibbo-model predictions for hyperon decay parameters and their experimental values[15] with the use of the $SU(2)_L\times SU(2)_R\times U(1)$ model. These have led to renewed interest in the search for RHC contributions in the experiments on muon decay by Carr *et al.*[16] and in the decay $K^{+}\to\mu^{+}\nu$ by Hayano *et al.*[17] These experiments have set new limits on polarization parameters and contributions due to the RHC factor.

Another field of activity in the domain of weak interactions in recent years has been to look for effects of finite neutrino mass,[18–25] mass mixings,[26–29] and neutrino oscillations.[25,30] In fact, a finite neutrino mass would require inclusion of RHC's in the theory.[5–8] As such, a systematic theory would require inclusion of all aspects appropriately.[14] As emphasized earlier, a search for contributions from RHC's, nonvanishing neutrino mass, and mass mixing even in low-energy leptonic and semileptonic processes could be useful. In fact, in our earlier discussion on K_{l3}^{+} decays,[29] it was shown that the effects of finite neutrino mass are substantial in all relevant parame-

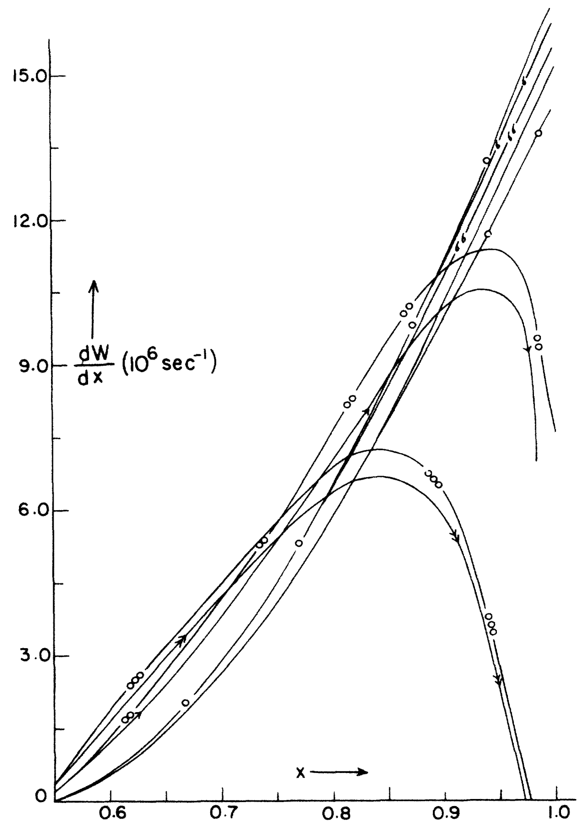

FIG. 1. Pion energy spectrum in K_{e3}^{+} decay. Solid, single-arrow, and double-arrow curves are for $m(\nu_3)=0$, 100, and 150 MeV, respectively, with LHC + WM. One-circle, two-circle, and three-circle (in gaps) curves are for $m(\nu_3)=0$, 100, and 150 MeV, respectively, with LHC + RHC + WM. One-σ and two-σ curves are for $m(\nu_3)=100$ and 150 MeV, respectively, with LHC + RHC + KM. Where one circle is on the line, the curve is for $m(\nu_3)=150$ MeV with LHC + KM. Curves for $m(\nu_3)=100$ and 150 MeV with LHC + HM, and LHC + RHC + HM, not shown in the figure, almost coincide with the curves for $m(\nu_3)=0$ with LHC + WM and LHC + RHC + WM, respectively. The curve for $m(\nu_3)=100$ MeV with LHC + KM, not shown in the figure, also almost coincides with the curve for $m(\nu_3)=0$ with LHC + WM.

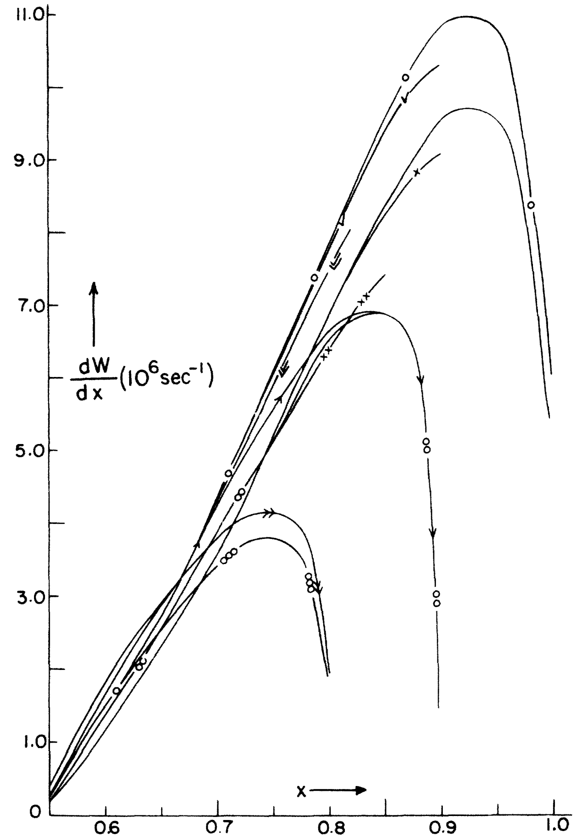

FIG. 2. Pion energy spectrum in $K_{\mu 3}^{+}$ decay. One-cross, two-cross curves and one-right-mark, two-right-mark curves are for $m(\nu_3)=100$ and 150 MeV with LHC + HM and LHC + RHC + HM, respectively. Curves for $m(\nu_3)=100$, 150 MeV with LHC + KM and LHC + RHC + KM, not shown in the figure, almost coincide with the corresponding curves for $m(\nu_3)=0$. Other descriptions of the curves are identical to those given in Fig. 1.

ters of the decay, and mixing effects show their presence in energy and angular correlations. We now report in this work our investigations on K_{l3}^{+} decays with the inclusion of RHC contributions, along with those of nonvanishing neutrino mass and mass mixings. At present, a K^{+} beam is copiously available at CERN in the p-$\bar{p}$ collider (LEAR) and as such this facility could possibly be made use of for investigating contributions from these factors to the various parameters pertaining to these decays.

The investigation deals with the following aspects of K_{l3}^{+} decays: (i) pion energy spectrum, (ii) decay probability, (iii) π-1 ($=e,\mu$) angular correlations, (iv) π-l energy correlations, (v) lepton energy spectrum, (vi) π-ν_i ($i=e,\mu,\tau$) angular correlations, (vii) π-ν_i energy correlations, (viii) l-ν_i angular correlations, (ix) l-ν_i energy correlations, (x) the ratio $R=W(K_{\mu 3}^{+})/W(K_{e3}^{+})$, and (xi) lepton longitudinal polarizations.

We use the RHC-factor contribution from the presently known limit of Ref. 17. The mixing used in the quark sector is of KM type whereas in the lepton sector we use KM[28] as well as hierarchical (H) mixings,[29] the latter being included for the purpose of comparison.

In the next section we give details of our discussion pertaining to all the aspects listed in (i)—(xi) and a summary of the conclusions is given in Sec. III.

II. K_{l3}^{+} DECAYS

A. Pion energy spectrum in $K^{+}\to l^{+}\nu_i\pi^{0}$

The matrix element for the processes $K^{+}\to l^{+}\nu_i\pi^{0}$, with the inclusion of RHC,[11] mixing matrices for neutrino species, and radiative correction,[31] is given by

$$M=\frac{G'}{\sqrt{2}}V_{12}C\sum_i |U_{li}|\bar{u}\nu_i[(p_K+p_\pi)f_+ +(p_K-p_\pi)f_-]$$
$$\times\gamma^{\lambda}[1-\gamma^5+F(1+\gamma^5)]v_l\ , \qquad (1)$$

where G' is the coupling constant inclusive of radiative correction, U_{li} are the elements of the neutrino mass mix-

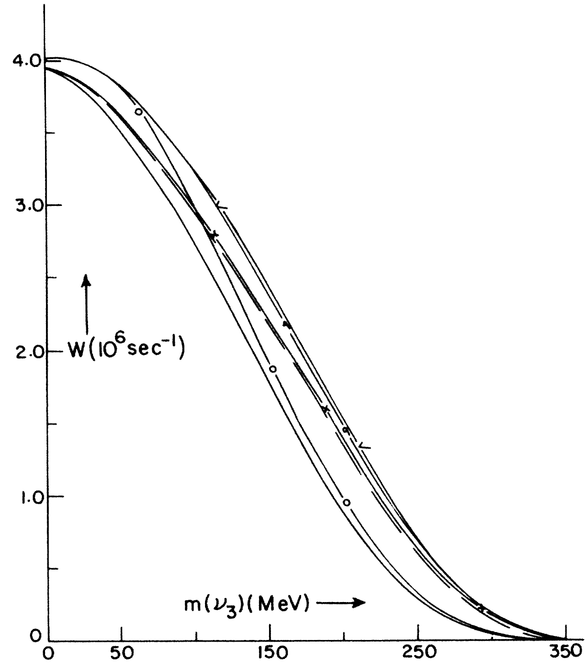

FIG. 3. Variation of decay probability with $m(\nu_3)$ in K_{e3}^+ decay. Solid curve, dashed curve, and cross curve are for LHC + WM, LHC + KM, and LHC + HM, respectively. One-circle, one-right-mark, and one-σ curves are for LHC + RHC + WM, LHC + RHC + HM, and LHC + RHC + KM, respectively.

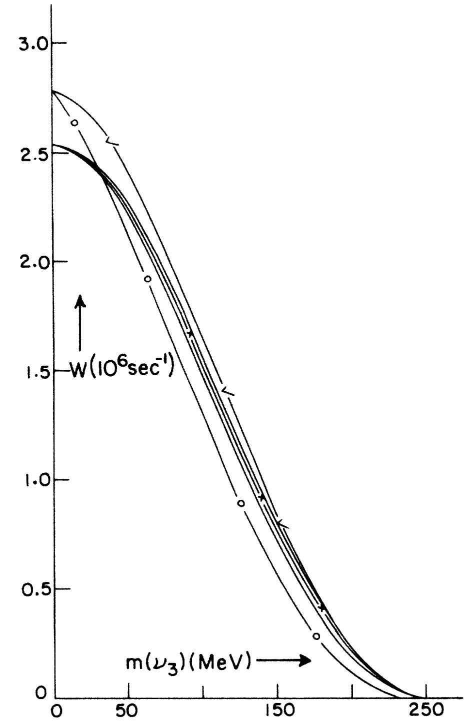

FIG. 4. Variation of decay probability with $m(\nu_3)$ in $K_{\mu 3}^+$ decay. The description of the curves is identical to that given in Fig. 3. The curve for LHC + RHC + KM, not shown in the figure, almost coincides with the curve for LHC + RHC + HM.

ing matrix with $l=e,\mu$ and $i=1,2,3$, V_{12} is the matrix element of the KM mixing matrix in the quark sector,[32,33] C is the Clebsch-Gordan coefficient,[31]

$$F=\frac{g_R{}^2 M_L{}^2 V_{12}{}^R}{g_L{}^2 M_R{}^2 V_{12}} ,$$

with $g_{L,R}$ being the coupling constants associated with the subgroups $SU(2)_{L,R}$, $M_{L,R}$ are the masses of the corresponding charged gauge bosons, and V_{12}^R is the KM mixing element in the RH-quark sector. Following Oka,[11] we assume that RH neutrinos are sufficiently light to participate in the decay. The matrix element, Eq. (1) of Ref. 29, is a special case of Eq. (1), when $F=0$.

The expression for the pion energy spectrum is given by

$$\begin{aligned}\frac{dW}{dx}=&\frac{C^2G'^2V_{12}{}^2\sum_i |U_{li}|^2 m_K{}^5(x^2-4\delta_\pi{}^2)^{1/2}\lambda^{1/2}((k-x),\delta_l{}^2,\delta_i{}^2)f_+{}^2}{384\pi^3(k-x)^3}\\&\times\Big((1+F^2)\{(x^2-4\delta_\pi{}^2)[2(k-x)^2-(k-x)(\delta_l{}^2+\delta_i{}^2)-(\delta_l{}^2-\delta_i{}^2)^2]+3[(k-x)(\delta_l{}^2+\delta_i{}^2)-(\delta_l{}^2-\delta_i{}^2)^2](1-\delta_\pi{}^2)^2\}\\&-12F(k-x)^2\delta_l\delta_i(k+x)+6R_e\xi(1-\delta_\pi{}^2)(k-x)\{(k-x)[(\delta_l{}^2+\delta_i{}^2)(1+F^2)-4F\delta_l\delta_i]-(\delta_l{}^2-\delta_i{}^2)^2(1+F^2)\}\\&+3|\xi|^2(k-x)^2\{(k-x)[(\delta_l{}^2+\delta_i{}^2)(1+F^2)-4F\delta_l\delta_i]-(\delta_l{}^2-\delta_i{}^2)^2(1+F^2)\}\Big) ,\end{aligned}\qquad(2)$$

where $G'^2=1.021G_\mu{}^2$ (Ref. 31), $C^2=\frac{1}{2}$ (Ref. 31),

$$x=\frac{2E_\pi}{m_K},\quad E_\pi=\text{energy of } \pi^0 ,$$

$$\delta_\pi{}^2=\frac{m_{\pi^0}{}^2}{m_K{}^2},\quad \delta_l{}^2=\frac{m_l{}^2}{m_K{}^2},\quad \delta_i{}^2=\frac{m^2(\nu_i)}{m_K{}^2} ,$$

$$k=1+\delta_\pi{}^2,\quad \lambda(x,y,z)=x^2+y^2+z^2-2(xy+yz+zx) ,$$

$$\xi=\frac{f_-}{f_+},\quad \xi(0)=\xi\left[1+\lambda_+\frac{q^2}{m_{\pi^0}{}^2}\right] ,$$

$$f_+=f_+(0)\left[1+\frac{\lambda_+q^2}{m_{\pi^0}{}^2}\right] ,$$

$$q^2=(p_K-p_\pi)^2$$

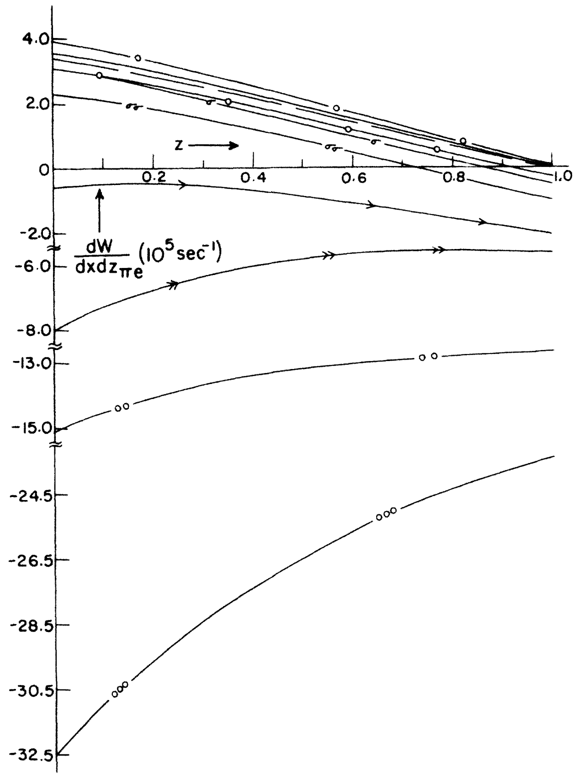

FIG. 5. π-e angular correlation in K_{e3}^{+} decay. Dashed curve is for $m(\nu_3)=100$ MeV with LHC + KM and the descriptions of the other curves are identical to those given in Fig. 1. Curves for $m(\nu_3)=100$ and 150 MeV with LHC + HM and LHC + RHC + HM, not shown in the figure, almost coincide with the corresponding curves for $m(\nu_3)=0$.

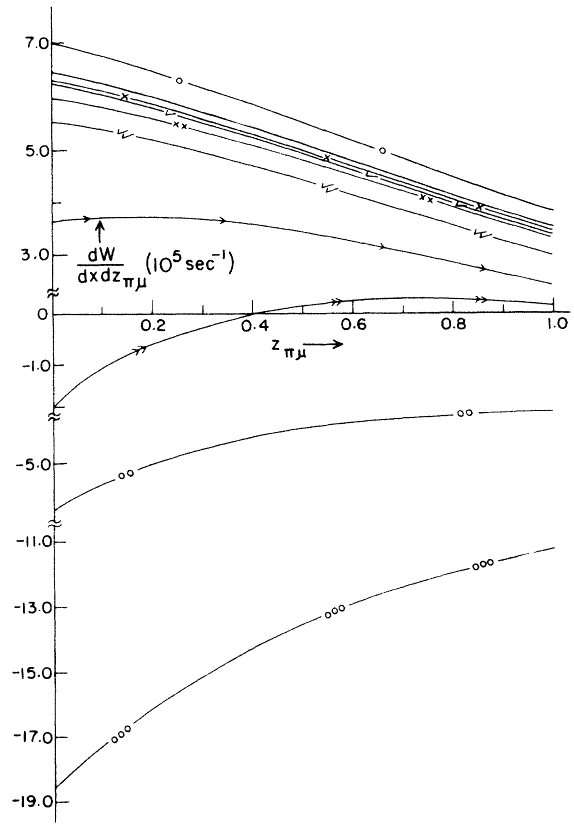

FIG. 6. π-μ angular correlation in $K_{\mu 3}^{+}$ decay. The description of the curves is identical to that given in Fig. 2. Curves for $m(\nu_3)=100$ and 150 MeV with LHC + KM and LHC + RHC + KM almost coincide with the corresponding curves for $m(\nu_3)=0$.

(see Refs. 34 and 35). For the purpose of calculations we take

$$f_{+}(0)V_{12}=0.2161$$

(see Ref. 31),

$$\xi(0)=0, \quad \lambda_{+}=0.029\pm0.004$$

for K_{e3}^{+} decays,[34] and

$$\lambda_{+}=0.032\pm0.008\ ,$$

$$\xi(0)=-0.35\pm0.15$$

for $K_{\mu 3}^{+}$ decays,[34]

$$F=0.295$$

(see Ref. 17). Expression (2) shows that, in general, the pion energy spectrum for $l=e$ or μ, will be the sum of three different spectra for the cases $i=1,2,3$. Confining to the three-neutrino world, and, in order to have an order-of-magnitude estimate, we adopt the convention that the neutrino masses $m(\nu_i)$ are in ascending order of values, i.e., $m_1<m_2<m_3$. Further, for the case of nondegenerate neutrinos, we take ν_1, ν_2, and ν_3 to be, respectively, ν_e, ν_u, and ν_τ. The use of the present experimental bounds on the masses of various neutrino species,[18–20] $20<m(\nu_e)<46$ eV, $m(\nu_\mu)<0.50$ MeV, and $m(\nu_\tau)<143$ MeV, gives $\delta_1<9.32\times10^{-8}$, $\delta_2<1.01\times10^{-3}$, and $\delta_3<0.30$, where $\delta_i=m(\nu_i)/m_K$. Thus the dominant contribution comes from δ_3 only. Retaining δ_3, we obtain for the pion energy spectrum, from Eq. (2), the expression

$$\frac{dW}{dx}=\frac{C^2G'^2V_{12}{}^2m_K{}^5(x^2-4\delta_\pi{}^2)^{1/2}f_{+}{}^2(0)}{384\pi^3(k-x)^3}\left[1+\frac{\lambda_{+}(k-x)}{\delta_\pi{}^2}\right]^2$$

$$\times\Bigg[(1-U_{l3}{}^2)(k-x-\delta_l{}^2)(1+F^2)$$

$$\times\Bigg\{(x^2-4\delta_\pi{}^2)[2(k-x)^2-(k-x)\delta_l{}^2-\delta_l{}^4]$$

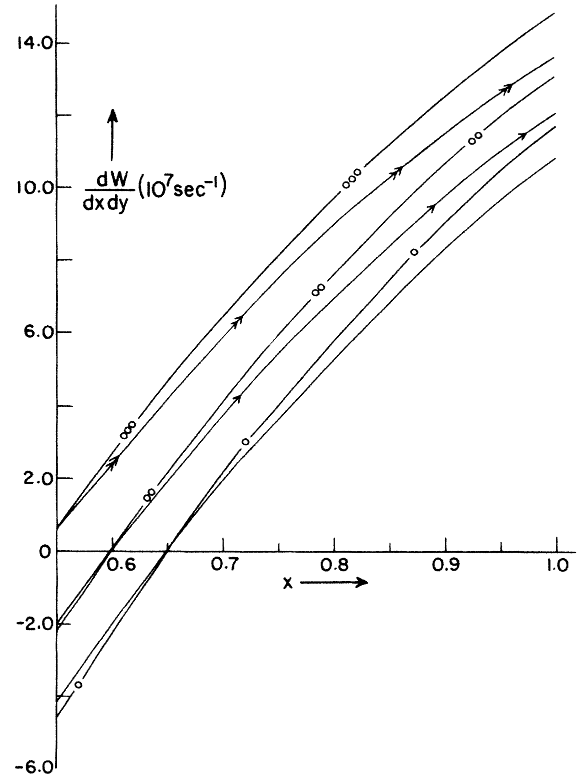

FIG. 7. π-e energy correlation in K_{e3}^+ decay. The description of the curves is identical to that given in Fig. 1. Curves for $m(\nu_3)=100$ and 150 MeV with LHC + KM, LHC + RHC + KM, and LHC + HM, LHC + RHC + HM, not shown in the figure, almost coincide with the corresponding curves for $m(\nu_3)=0$.

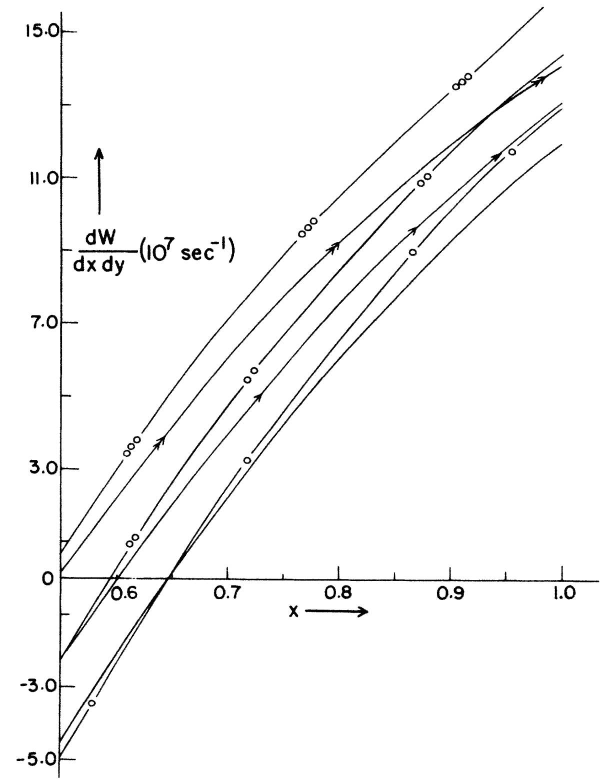

FIG. 8. π-μ energy correlation in $K_{\mu 3}^+$ decay. The description of the curves is identical to that given in Fig. 1. Curves for $m(\nu_3)=100$ and 150 MeV with LHC + KM, LHC + RHC + KM, and LHC + HM, LHC + RHC + HM, not shown in the figure, almost coincide with the corresponding curves for $m(\nu_3)=0$.

$$
\begin{aligned}
&+3\delta_l^2(k-x-\delta_l^2)\left\{(1-\delta_\pi^2)^2+(k-x)\left[(1-\delta_\pi^2)2\xi(0)\left[1-\frac{\lambda_+(k-x)}{\delta_\pi^2}\right]\right.\right.\\
&\qquad\qquad\left.\left.+\xi^2(0)\left[1-\frac{\lambda_+(k-x)}{\delta_\pi^2}\right]^2(k-x)\right]\right\}\Bigg]\\
&+U_{l3}^2\lambda^{1/2}((k-x),\delta_l^2,\delta_3^2)\Bigg[(1+F^2)\{(x^2-4\delta_\pi^2)[2(k-x)^2-(k-x)(\delta_l^2+\delta_3^2)-(\delta_l^2-\delta_3^2)^2]\\
&\qquad\qquad+3[(k-x)(\delta_l^2+\delta_3^2)-(\delta_l^2-\delta_3^2)^2](1-\delta_\pi^2)^2\}\\
&\qquad-12F(k-x)^2\delta_l\delta_3(k+x)\\
&\qquad+6\xi(0)\left[1-\frac{\lambda_+(k-x)}{\delta_\pi^2}\right](1-\delta_\pi^2)(k-x)\\
&\qquad\times\{(k-x)[(\delta_l^2+\delta_3^2)(1+F^2)-4F\delta_l\delta_3]-(\delta_l^2-\delta_3^2)^2(1+F^2)\}\\
&\qquad+3\xi^2(0)\left[1-\frac{\lambda_+(k-x)}{\delta_\pi^2}\right]^2(k-x)^2\,\{(k-x)[(\delta_l^2+\delta_3^2)(1+F^2)-4F\delta_l\delta_3]\\
&\qquad\qquad\left.-(\delta_l^2-\delta_3^2)^2(1+F^2)\}\right]\Bigg]\,. \qquad (3)
\end{aligned}
$$

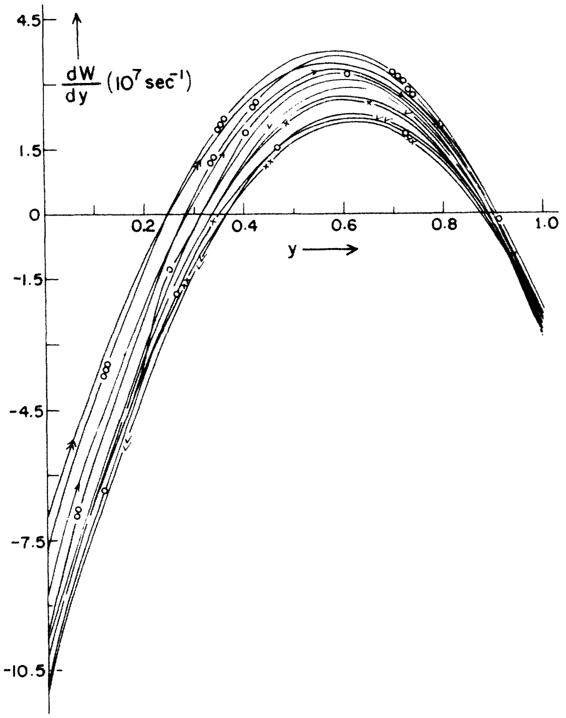

FIG. 9. Electron energy spectrum in K_{e3}^+ decay. The dashed curve and the curve with a circle on line are for $m(\nu_3)=100$ and 150 MeV with LHC + KM, respectively, and the description of the other curves is identical to that given in Fig. 2. Curves for $m(\nu_3)=100$ and 150 MeV with LHC + RHC + KM, not shown in the figure, almost coincide with the corresponding curves for HM.

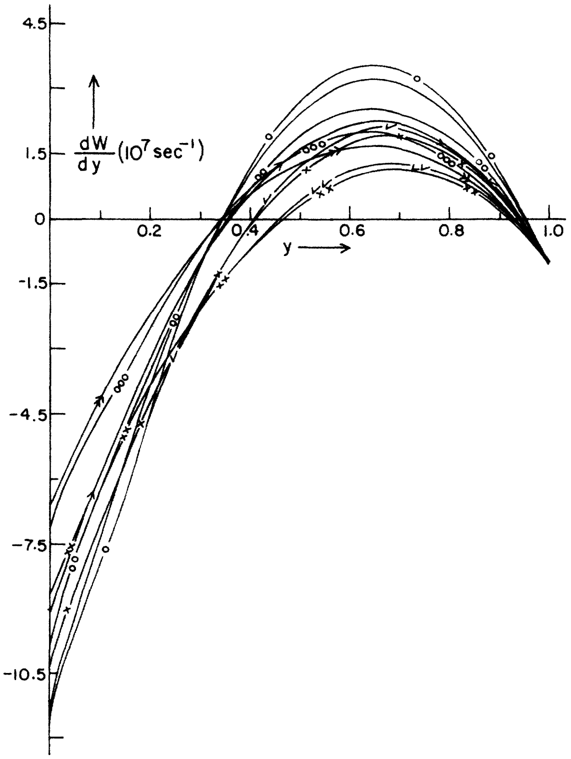

FIG. 10. Muon energy spectrum in $K_{\mu 3}^+$ decay. The description of the curves is identical to that given in Fig. 2. Curves for $M(\nu_3)=100$ and 150 MeV with LHC + KM, LHC + RHC + KM, not shown in the figure, almost coincide with the corresponding curves for HM.

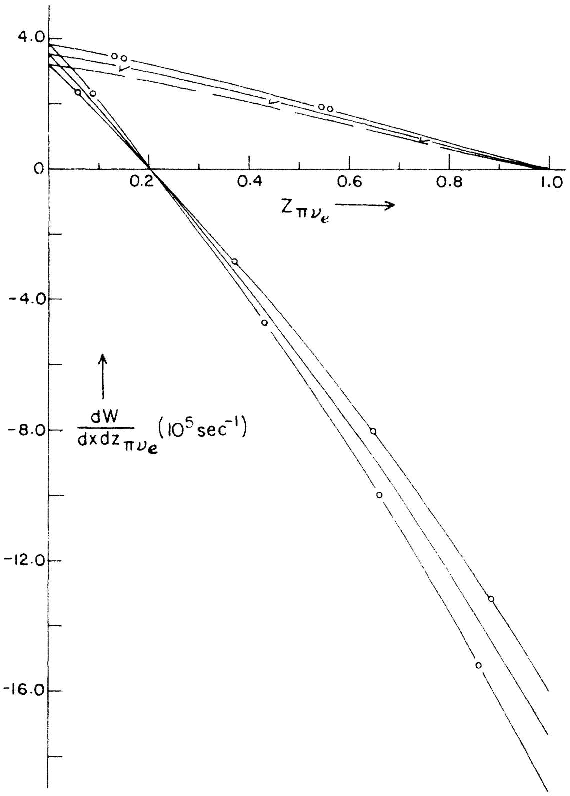

FIG. 11. π-ν_e angular correlation in K_{e3}^+ decay. The solid and one-circle curves are for LHC + WM and LHC + RHC + WM, respectively, with $y_{\max}$. The one-right-mark and two-circle curves are for LHC + WM, and LHC + RHC + WM, respectively, with $y_{\min}$. The dashed curve is for LHC + KM with $y_{\min}$ and a circle-on-line curve is for LHC + KM with $y_{\max}$. Curves for LHC + RHC + KM with both $y_{\max}$ and $y_{\min}$, not shown in the figure, almost coincide with the corresponding curves for WM.

A plot of the pion energy spectrum, in the K_{e3}^+ decay, is shown in the Fig. 1 for $m(\nu_3)=0$, 100, and 150 MeV. Equations (4) and (5) of Ref. 29 are used, respectively, for hierarchical[36] and KM (Ref. 28) mixings.

The pion energy spectrum with both left-handed and right-handed currents (LHC + RHC) for the case without mixing (WM) is distinct from the corresponding one not involving RHC's over almost the entire range of x. The RHC contribution enhances relatively the value of dW/dx over almost the entire range of x. The same pattern follows for the finite-neutrino-mass cases $m(\nu_3)=100$, 150 MeV. Mixing contributions are, however, not distinct except for $x>0.9$.

The pion energy spectrum in $K_{\mu 3}^+$ decay is shown in Fig. 2. The energy spectrum for the LHC + WM with $m(\nu_3)=0$ case differs distinctly from that of LHC + RHC + WM with $m(\nu_3)=0$ and takes higher values of dW/dx for all values of x. But for finite $m(\nu_3)=100$ or 150 MeV (WM) the two are not distinct over the entire range of x. The curves involving hierarch-

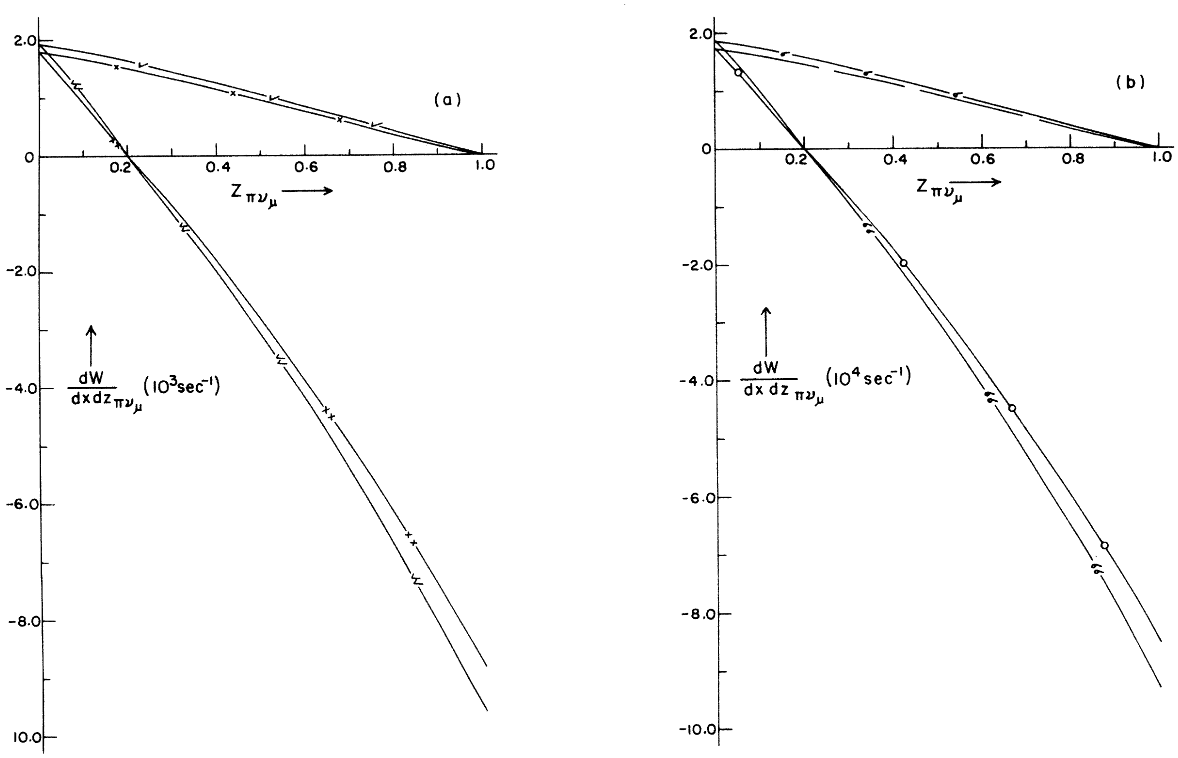

FIG. 12. (a) π-ν_μ angular correlation in K_{e3}^+ decay with HM. The one-right-mark and one-cross curves are for LHC + RHC and LHC, respectively, with $y_{\min}$. Two-cross and two-right-mark curves are for LHC and LHC + RHC, respectively, with $y_{\max}$. Two-cross and two-right-mark curves are for LHC and LHC + RHC, respectively, with $y_{\max}$. (b) π-ν_μ angular correlation in K_{e3}^+ with KM. The dashed and one-σ curves are for LHC and LHC + RHC, respectively, with $y_{\min}$. The curve with one circle on line and the two-σ curve are for LHC and LHC + RHC, respectively, with $y_{\max}$.

ical mixings (HM) are, however, discernible from the corresponding WM curves. An unambiguous conclusion is that the RHC contribution enhances relatively the value of dW/dx for all values of x.

B. Decay probability

The expression for the decay probability obtained by integrating Eq. (3) is given by

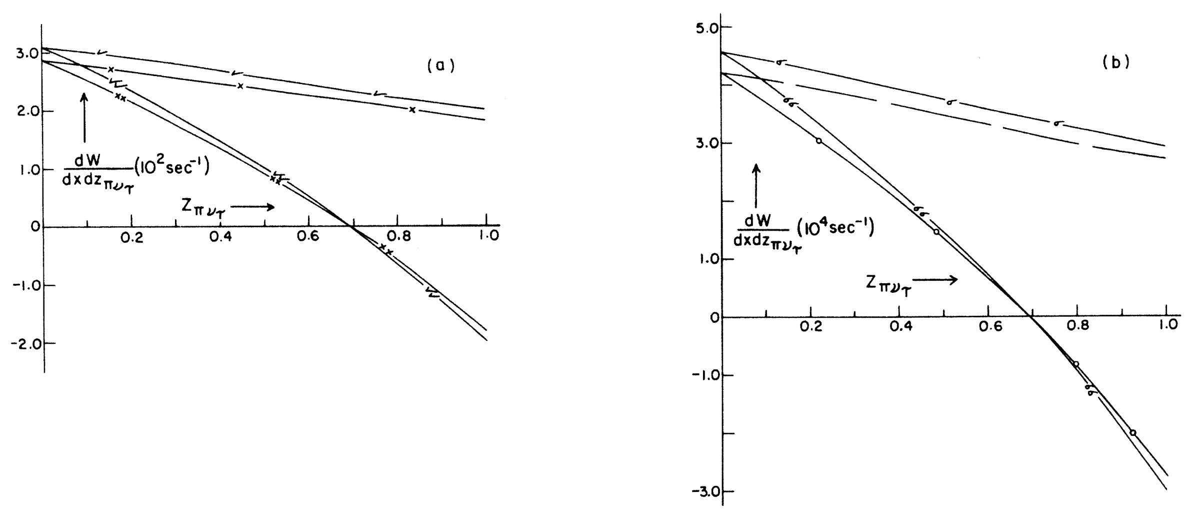

FIG. 13. π-ν_τ angular correlation in K_{e3}^+ decay with (a) HM, and (b) KM. The description of the curves is identical to that given in Figs. 12(a) and 12(b).

$$
\begin{aligned}
W=\frac{G'^2V_{12}^2m_K^5C^2}{384\pi^3}\int_{x_{\min}}^{x_{\max}} & \frac{(x^2-4\delta_\pi^2)^{1/2}f_+^2(0)}{(k-x)^3}\left[1+\frac{\lambda_+(k-x)}{\delta_\pi^2}\right]^2 \\
& \times\Bigg[(1-U_{l3}^2)(k-x-\delta_l^2)(1+F^2) \\
& \quad\times\Bigg\{(x^2-4\delta_\pi^2)[2(k-x)^2-(k-x)\delta_l^2-\delta_l^4] \\
& \quad+3\delta_l^2(k-x-\delta_l^2)\Bigg\{(1-\delta_\pi^2)^2+(k-x)\Bigg[2\xi(0)\left[1-\frac{\lambda_+(k-x)}{\delta_\pi^2}\right](1-\delta_\pi^2) \\
& \quad+\xi^2(0)\left[1-\frac{\lambda_+(k-x)}{\delta_\pi^2}\right]^2(k-x)\Bigg]\Bigg\}\Bigg\} \\
& +U_{l3}^2\lambda^{1/2}((k-x),\delta_l^2,\delta_3^2)\Bigg[(1+F^2)\{(x^2-4\delta_\pi^2)[2(k-x)^2-(k-x)(\delta_l^2+\delta_3^2) \\
& \quad-(\delta_l^2-\delta_3^2)^2] \\
& \quad+3[(k-x)(\delta_l^2+\delta_3^2)-(\delta_l^2-\delta_3^2)^2](1-\delta_\pi^2)^2\} \\
& \quad-12F(k-x)^2\delta_l\delta_3(k+x) \\
& \quad+6\xi(0)\left[1-\frac{\lambda_+(k-x)}{\delta_\pi^2}\right](1-\delta_\pi^2)(k-x) \\
& \quad\times\{(k-x)[(\delta_l^2+\delta_3^2)(1+F^2)-4F\delta_l\delta_3]-(\delta_l^2-\delta_3^2) \\
& \quad\times(1+F^2)\}+3\xi^2(0)\left[1-\frac{\lambda_+(k-x)}{\delta_\pi^2}\right]^2(K-x)^2 \\
& \quad\times\{(K-x)[(\delta_l^2+\delta_3^2)(1+F^2) \\
& \quad-4F\delta_l\delta_3] \\
& \quad-(\delta_l^2-\delta_3^2)^2(1+F^2)\}\Bigg]\Bigg]dx\,, \qquad (4)
\end{aligned}
$$

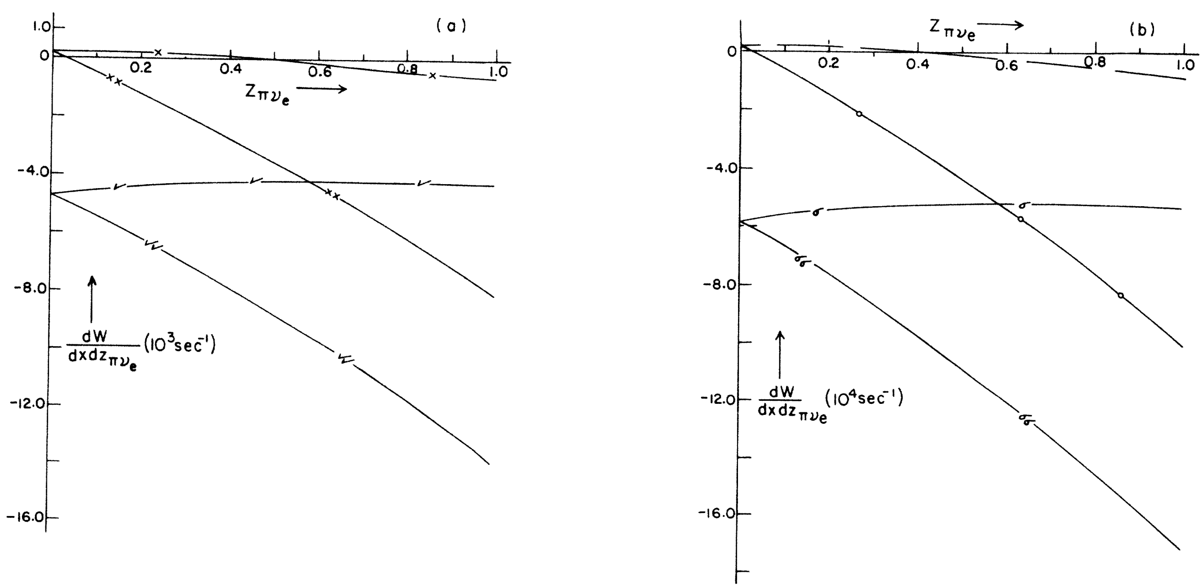

FIG. 14. π-ν_e angular correlation in $K_{\mu 3}^+$ decay with (a) HM, and (b) KM. The description of the curves is identical to that given in Figs. 12(a) and 12(b).

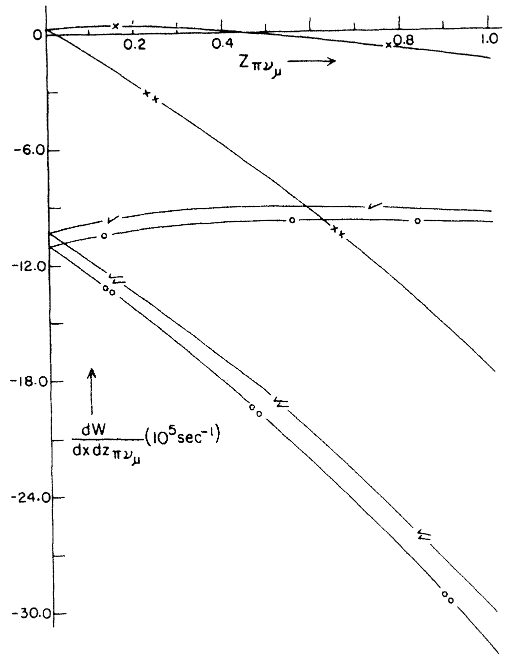

FIG. 15. π-ν_μ angular correlation in $K_{\mu3}^+$ decay. One-circle and two-circles curves are for LHC + RHC + WM with y_{max} and y_{min}, respectively. The description of the other curves is identical to that given in Fig. 12(a). Curves for LHC + WM with y_{max} and y_{min}, and LHC + KM, LHC + RHC + KM, not shown in the figure, almost coincide with the corresponding curves of HM, respectively.

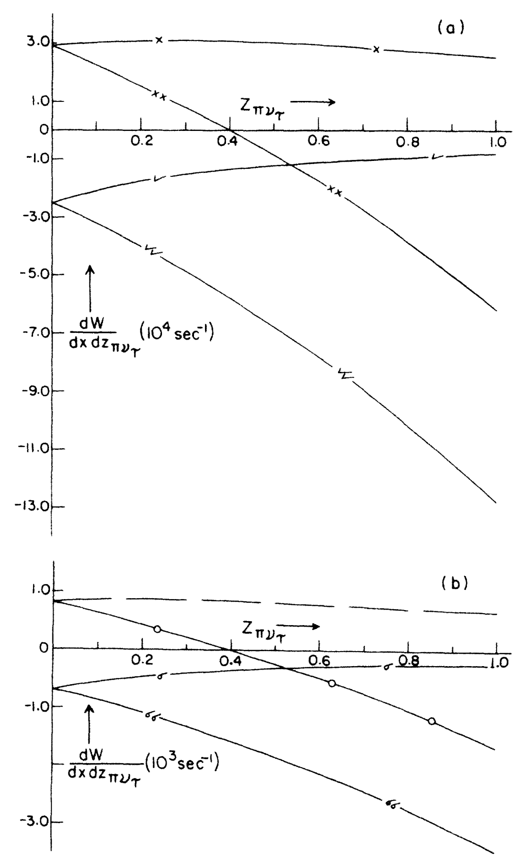

FIG. 16. π-ν_τ angular correlation in $K_{\mu3}^+$ decay with (a) HM and (b) KM. The description of the curves is identical to that given in Figs. 12(a) and 12(b).

where

$$x_{max} = \frac{m_K{}^2 + m_{\pi^0}{}^2 - [m_l + m(\nu_i)]^2}{m_K{}^2} ,$$

and

$$x_{min} = \frac{2m_{\pi^0}}{m_K} . \qquad (5)$$

Variation of the decay probability of K_{e3}^+ decay with finite $m(\nu_3)$ is shown in Fig. 3. The LHC + RHC with WM curve lies above the LHC + WM curve almost over the entire range of $m(\nu_3)$. A similar conclusion follows when H mixing is included. But for KM mixing the RHC contribution cannot be easily separated. It may thus enable the distinction between types of mixings. Using $W_{expt}(K_{e3}^+) = (3.9 \pm 0.041) \times 10^6$ sec^{-1} (Ref. 34), and the procedure of Ref. 29, we calculate the value $m(\nu_3)$ in LHC and LHC + RHC cases for which theoretical and experimental values of $W(K_{e3}^+)$ become equal. The values of $m(\nu_3)$ so obtained are given in Table I.

Variation of the $K_{\mu3}^+$ decay probability with finite $m(\nu_3)$ is shown in Fig. 4. The curve corresponding to LHC + RHC + WM lies above the LHC + WM curve up to $m(\nu_3) = 40$ MeV, and thereafter it reduces and goes below this curve. As such, the RHC contribution is not unambiguous over the entire range of $m(\nu_3)$. The curve LHC + RHC + HM lies above the LHC + HM curve through the entire range of $m(\nu_3)$, enabling a precise distinction of the RHC contribution. Distinction between HM and KM mixings is not possible. Using

$$W_{expt}(K_{\mu3}^+) = (2.59 \pm 0.07) \times 10^6 \text{ sec}^{-1}$$

(Ref. 34), and the procedure of Ref. 29, we calculate $m(\nu_3)$ mass limits which are given in Table I.

It may, however, be emphasized that the experimental value of decay probabilities in these decays cannot be explained without introducing the RHC contribution without or with a finite neutrino mass $m(\nu_3)$. The upper limits on the RHC factor F obtained are <0.26 and <0.22, respectively, for K_{e3}^+ and $K_{\mu3}^+$ decays which are consistent with the value of the RHC factor of Ref. 17.

C. π-l angular correlations

The expression for the π-l angular correlations with the inclusion of RHC's and retention of dominant δ_3 terms is given below,

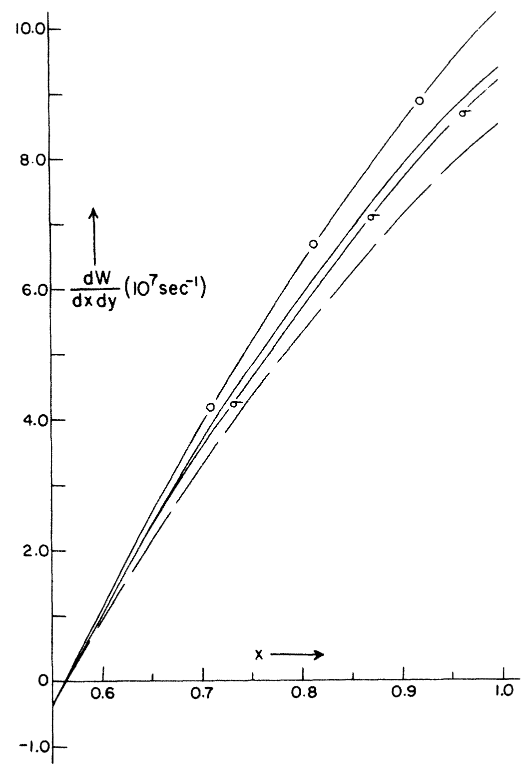

FIG. 17. π-ν_e energy correlation in K_{e3}^+ decay. The solid and one-circle, curves are for LHC + WM, and LHC + RHC + WM, respectively. The dashed and one-σ curves are for LHC + KM and LHC + RHC + KM, respectively. Curves for LHC + HM and LHC + RHC + HM, not shown in the figure, almost coincide with the curves for LHC + WM and LHC + RHC + WM, respectively.

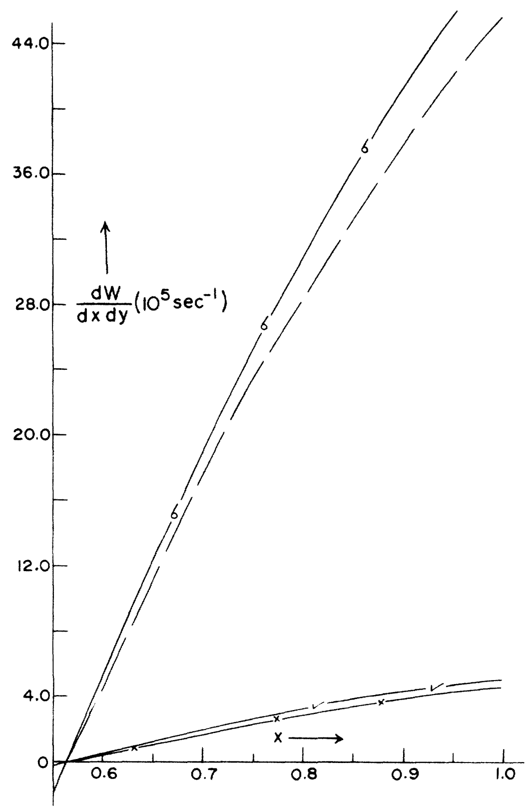

FIG. 18. π-ν_μ energy correlation in K_{e3}^+ decay. One-cross and one-right-mark curves are for LHC + HM and LHC + RHC + HM, respectively. The description of other curves is identical to that given in Fig. 17.

$$
\begin{aligned}
\frac{dW}{dx\,dz} = {} & \frac{C^2G'^2V_{12}^2m_K^5(x^2-4\delta_\pi^2)^{1/2}(y_1^2-4\delta_l^2)f_+^2(0)}{512\pi^3[(2-x)(y_1^2-4\delta_l^2)^{1/2}+(x^2-4\delta_\pi^2)^{1/2}yz]}\left[1+\frac{\lambda_+(k-x)}{\delta_\pi^2}\right]^2(1-U_{l3}^2)(1+F^2) \\
& \times\Bigg[[(2+x)(1-\delta_\pi^2)+(x^2-4\delta_\pi^2)]2y_1-y_1^2(2+x)^2 \\
& +(x^2-4\delta_\pi^2)^{1/2}(y_1^2-4\delta_l^2)^{1/2}2z[y_1(2+x)-(3-\delta_\pi^2+x)]-(x^2-4\delta_\pi^2)(y_1^2-4\delta_l^2)z^2 \\
& +8\delta_l^2(k+x)+2\xi(0)\left[1-\frac{\lambda_+(k-x)}{\delta_\pi^2}\right] \\
& \times[(2+x)(k-x)2y_1-y_1^2(4-x^2)-(x^2-4\delta_\pi^2)^{1/2}(y_1^2-4\delta_l^2)^{1/2}2z(xy_1+k-x) \\
& +(y_1^2-4\delta_l^2)(x^2-4\delta_\pi^2)z^2+8\delta_l^2(1-\delta_\pi^2)]+\xi^2(0)\left[1-\frac{\lambda_+(k-x)}{\delta_\pi^2}\right]^2 \\
& \times\{(2-x)(k-x)2y_1-y_1^2(2-x)^2-(x^2-4\delta_\pi^2)^{1/2}(y_1^2-4\delta_l^2)^{1/2}2z[(2-x)y_1-k+x] \\
& -(x^2-4\delta_\pi^2)(y_1^2-4\delta_l^2)z^2+8\delta_l^2(k-x)\}\Bigg]
\end{aligned}
$$

TABLE I. Values of $m(\nu_3)$ in K_{l3}^+ decays, calculated from decay probabilities with the inclusion of LHC + RHC and LHC, respectively.

Decay mode	Currents	$m(\nu_3)$ (MeV) Hierarchical mixing	KM mixing	Without mixing
1. K_{e3}^+	LHC + RHC	40±6	40±7	44±5
	LHC			
2. $K_{\mu 3}^+$	LHC + RHC	35±8	36±8	20±8
	LHC	15	15	14

TABLE II. Values of $m(\nu_3)$ in K_{l3}^+ decays, calculated from the ratio $R = W(K_{\mu 3}^+)/W(K_{e3}^+)$.

Currents	$m(\nu_3)$ (MeV) Hierarchical mixing	KM mixing	Without mixing
1. LHC + RHC	31±16	35±15	14±8
2. LHC	35±15	35±15	26±8

$$+\frac{C^2G'^2V_{12}^2m_K^5(x^2-4\delta_\pi^2)^{1/2}(y^2-4\delta_l^2)^{1/2}f_+^2(0)}{512\pi^3[(2-x)(y^2-4\delta_l^2)^{1/2}+(x^2-4\delta_\pi^2)^{1/2}yz]}\left[1+\frac{\lambda_+(k-x)}{\delta_\pi^2}\right]^2$$

$$\times U_{l3}^2\Bigg\{(1+F^2)\text{ (the quantity in the large square brackets with the replacement } y_1\to y)$$

$$-32F\delta_l\delta_3\left[k+x+2\xi(0)\left[1-\frac{\lambda_+(k-x)}{\delta_\pi^2}\right](1-\delta_\pi^2)+\xi^2(0)\left[1-\frac{\lambda_+(k-x)}{\delta_\pi^2}\right]^2(k-x)\right]\Bigg\}, \quad (6)$$

where

$$y_1=\frac{2((k+\delta_l^2-x)(2-x)-(x^2-4\delta_\pi^2)^{1/2}z\{(k+\delta_l^2-x)^2-\delta_l^2[(2-x)^2-(x^2-4\delta_\pi^2)z^2]\}^{1/2})}{(2-x)^2-(x^2-4\delta_\pi^2)z^2}$$

and (7)

$$y=\frac{2((k+\delta_l^2-\delta_3^2-x)(2-x)-(x^2-4\delta_\pi^2)^{1/2}z\{(k+\delta_l^2-\delta_3^2-x)^2-\delta_l^2[(2-x)^2-(x^2-4\delta_\pi^2)z^2]\}^{1/2})}{(2-x)^2-(x^2-4\delta_\pi^2)z^2}.$$

The π-e angular correlation in K_{e3}^+ decay is shown in Fig. 5 for $m(\nu_3)=0$, 100, and 150 MeV. The curve for LHC + RHC + WM with $m(\nu_3)=0$ lies above the corresponding curve of LHC + WM with $m(\nu_3)=0$. When a finite neutrino mass $m(\nu_3)$ (=100, 150 MeV) is included, the behavior is reversed for WM as well as for KM mixing cases. The RHC contribution is transparent for all cases. The general features of π-μ angular correlations (Fig. 6) in $K_{\mu 3}^+$ decay are identical to those of π-e correlations except for differences in numerical values.

D. π-l energy correlations

The expression for π-l energy correlation, with the inclusion of RHC and δ_3 dominance, is given by

$$\frac{dW}{dx\,dy}=\frac{C^2G'^2V_{12}^2m_K^5f_+^2(0)}{128\pi^3}\left[1+\frac{\lambda_+(k-x)}{\delta_\pi^2}\right]^2$$

$$\times\Bigg\{(1+F^2)(1-U_{l3}^2)\Bigg[[(2+x)(1-\delta_\pi^2)+(x^2-4\delta_\pi^2)]2y-y^2(2+x)^2$$

$$+[2(k-x+\delta_l^2)-y(2-x)][y(6+x)-2(4+\delta_l^2)]+8\delta_l^2(k+x)$$

$$+2\xi(0)\left[1-\frac{\lambda_+(k-x)}{\delta_\pi^2}\right]\{2y(2+x)(k-x)-y^2(4-x^2)$$

$$+[2(k-x+\delta_l^2)-y(2-x)](2\delta_l^2-xy-2y)+8\delta_l^2(1-\delta_\pi^2)\}$$

$$+\xi^2(0)\left[1-\frac{\lambda_+(k-x)}{\delta_\pi^2}\right]^2\{(k-x)(2-x)2y-y^2(2-x)^2$$

$$+[2(k-x+\delta_l^2)-y(2-x)](xy-4y+2\delta_l^2)+8\delta_l^2(k-x)\}\Bigg]$$

$$+(1+F^2)U_{l3}^2\Bigg[[(2+x)(1-\delta_\pi^2)+(x^2-4\delta_\pi^2)]2y-y^2(2+x)^2$$

$$+[2(k-x+\delta_l^2-\delta_3^2)-y(2-x)][y(6+x)-2(4+\delta_l^2-\delta_3^2)]$$

$$+8\delta_l^2(k+x)+2\xi(0)\left[1-\frac{\lambda_+(k-x)}{\delta_\pi^2}\right]$$

$$\times\{2y(2+x)(k-x)-y^2(4-x^2)+[2(k-x+\delta_l^2-\delta_3^2)-y(2-x)]$$

$$\times(2\delta_l^2-2\delta_3^2-xy-2y)+8\delta_l^2(1-\delta_\pi^2)\}$$

$$+\xi^2(0)\left[1-\frac{\lambda_+(K-x)}{\delta_\pi^2}\right]^2\{(k-x)(2-x)2y-y^2(2-x)^2$$

$$+[2(k-x+\delta_l^2-\delta_3^2)-y(2-x)]$$

$$\times(xy-4y+2\delta_l^2+2\delta_3^2)+8\delta_l^2(k-x)\}\Bigg]$$

$$-4FU_{l3}^2\delta_l\delta_3\left[k+x+2\xi(0)\left[1-\frac{\lambda_+(k-x)}{\delta_\pi^2}\right](1-\delta_\pi^2)+\xi^2(0)\left[1-\frac{\lambda_+(k-x)}{\delta_\pi^2}\right]^2(k-x)\right]\Bigg\}, \quad (8)$$

with

$$x=2E_\pi/m_K,\quad y=2E_l/m_K\ . \quad (9)$$

π-e energy correlations in the decay K_{e3}^+ are shown in Fig. 7 for $y=0.5$. All curves involving the RHC contribution lie above the corresponding ones not involving the RHC excepting for low values of x. Thus, the RHC contribution as well as those involving finite $m(\nu_3)$ can be distinguished. Types of mixings are, however, indistinguishable. Identical conclusions follow in the π-μ energy correlation in the $K_{\mu3}^+$ decay (Fig. 8).

E. Lepton energy spectrum in K_{l3}^+ decays

Integration of Eq. (8) for x gives the expression for lepton energy spectrum dW/dy. The limits of integration, used for x, are those given in Eq. (5). Variation of dW/dy with y, for $l=e$, is shown in Fig. 9.

It is not possible to distinguish between curves involving LHC + RHC + WM with $m(\nu_3)=0$, 100, and 150 MeV from the corresponding ones not involving the RHC over the entire range of y, except for $0.5<y<0.7$. However, curves involving a finite $m(\nu_3)$ with or without the RHC contribution are distinguishable from those having $m(\nu_3)=0$ and different $m(\nu_3)$ values. Mixing effects are also not precisely discernible from the corresponding WM cases.

The general features of the muon energy spectrum in $K_{\mu3}^+$ decay (Fig. 10) are identical to those of the electron energy spectrum. In this spectrum the curves involving a finite neutrino mass lie below the curves of LHC + RHC + WM and LHC + WM, with $m(\nu_3)=0$ in the positive region of the spectrum.

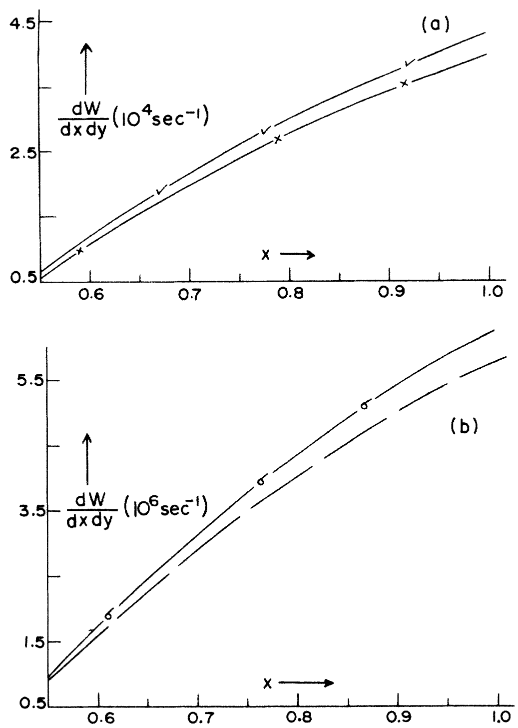

FIG. 19. π-ν_τ energy correlation in K_{e3}^+ decay with (a) HM and (b) KM. The description of the curves is identical to that given in Figs. 18 and 17.

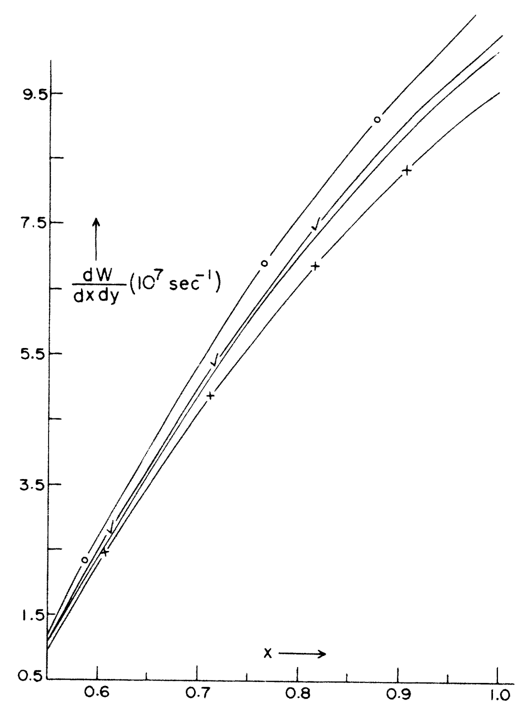

FIG. 21. π-ν_μ energy correlation in $K_{\mu 3}^+$ decay. The description of the curves is identical to that given in Figs. 17 and 18.

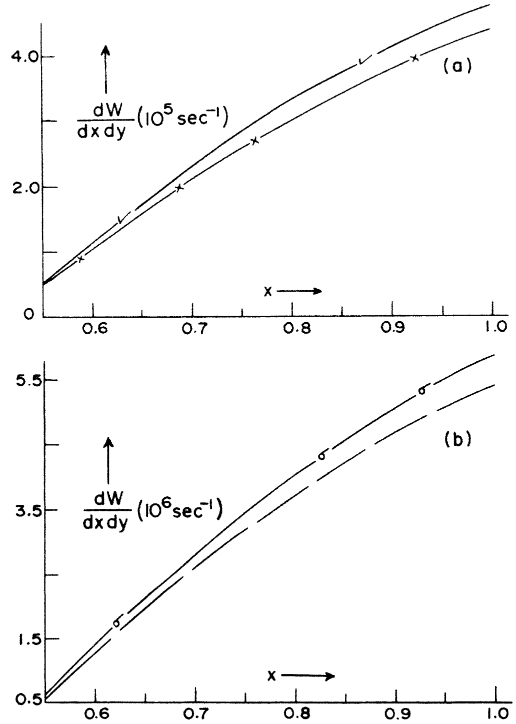

FIG. 20. π-ν_e energy correlation in $K_{\mu 3}^+$ decay with (a) HM and (b) KM. The description of the curves is identical to that given in Figs. 18 and 17.

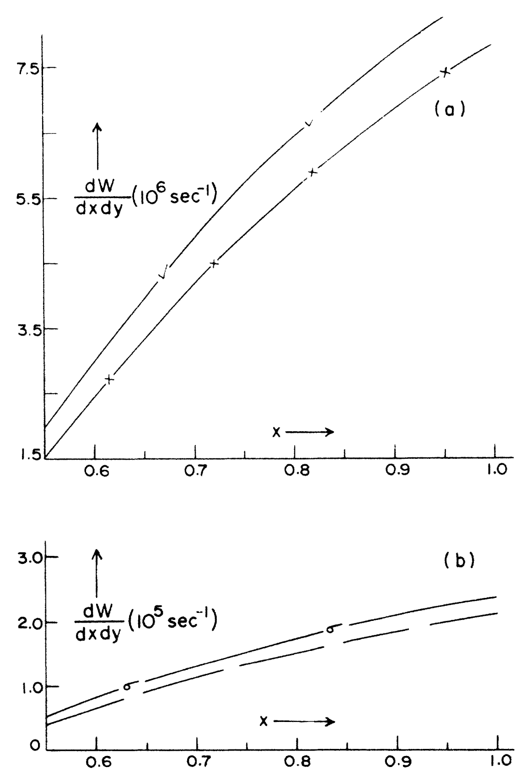

FIG. 22. π-ν_τ energy correlation in $K_{\mu 3}^+$ decay with (a) HM and (b) KM. The description of the curves is identical to that given in Figs. 18 and 17.

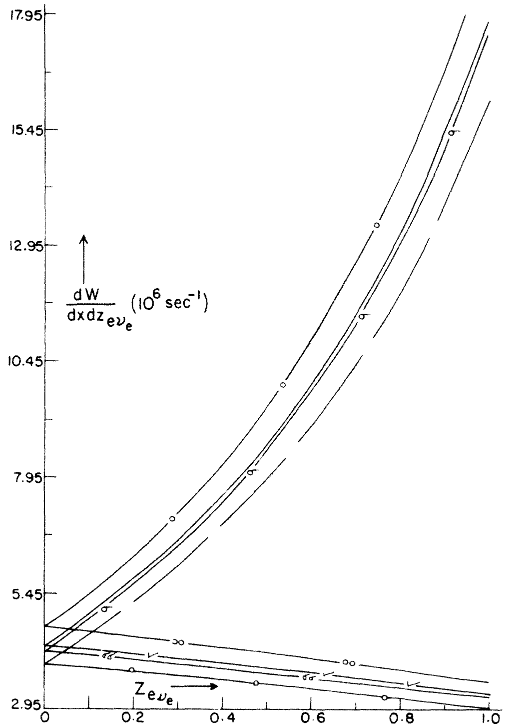

FIG. 23. e-ν_e angular correlation in K_{e3}^+ decay. The solid and one-circle curves are for LHC + WM and LHC + RHC + WM, respectively, with y_{max}. The one-right-mark and two-circle curves are for LHC + WM and LHC + RHC + WM, respectively, with y_{min}. The dashed and one-σ curves are for LHC + KM and LHC + RHC + KM, respectively, with y_{max}. The curve with one circle on line and the two-σ curve are for LHC + KM and LHC + RHC + KM, respectively, with y_{min}. Curves for LHC + HM, LHC + RHC + HM with y_{max} and y_{min}, not shown in the figure, almost coincide with the corresponding curves of WM.

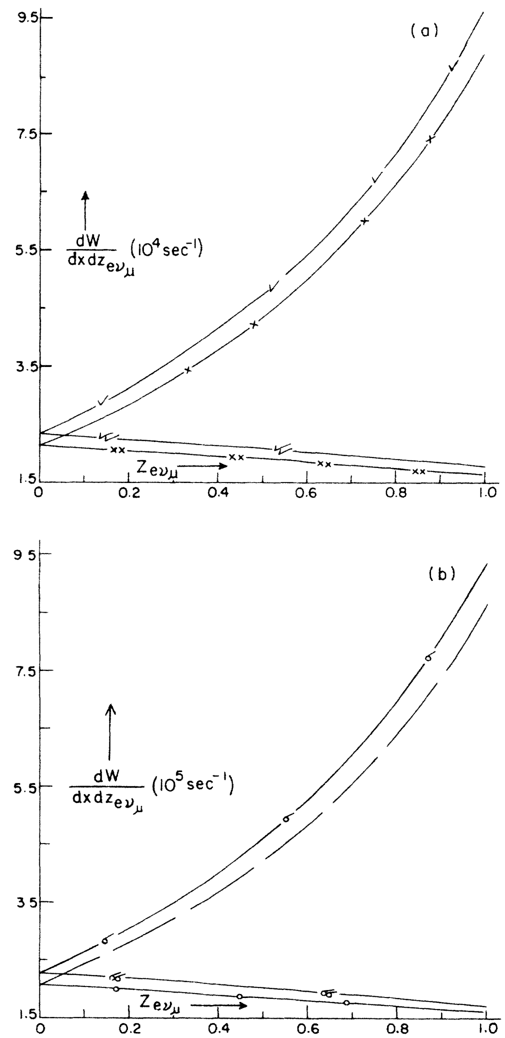

FIG. 24. (a) e-ν_μ angular correlation in K_{e3}^+ decay with HM. The one-cross and one-right-mark curves are for LHC + HM and LHC + RHC + HM, respectively, with y_{max}. Two-cross and two-right-mark curves are for LHC + HM and LHC + RHC + HM, respectively, with y_{min}. (b) e-ν_μ angular correlation in K_{e3}^+ decay, with KM. The description of the curves is identical to that given in Fig. 23.

F. π-ν_i angular correlations in K_{l3}^+ decays

The expressions for pion-neutrino angular correlations are obtained from the expressions of π-l angular correlations, Eq. (6), by making the replacements $m_l \leftrightarrow m(\nu_i)$, $E_l \rightarrow E(\nu_i)$, $\theta_{\pi l} \rightarrow \theta_{\pi\nu_i}$, and $\sum_{i=1}^{3} |U_{li}|^2 = |U_{li}|^2$:

$$
\begin{aligned}
\frac{dW}{dx\,dz} = {} & C^2 \frac{|U_{li}|^2 G'^2 V_{12}^2 m_K^5 (x^2-4\delta_\pi^2)^{1/2}(y^2-4\delta_i^2)^{1/2} f_+^2(0)}{512\pi^3[(2-x)(y^2-4\delta_i^2)^{1/2}+(x^2-4\delta_\pi^2)^{1/2}yz]} \left[1+\frac{\lambda_+(k-x)}{\delta_\pi^2}\right]^2 \\
& \times \left\{ \left\{ [(2+x)(1-\delta_\pi^2)+(x^2-4\delta_\pi^2)]2y - y^2(2+x)^2 + 2(x^2-4\delta_\pi^2)^{1/2}(y^2-4\delta_i^2)^{1/2} z[y(2+x)-3+\delta_\pi^2-x] \right.\right. \\
& \quad - (x^2-4\delta_\pi^2)(y^2-4\delta_i^2)z^2 + 8\delta_i^2(k+x) \\
& \quad + 2\xi(0)\left[1-\frac{\lambda_+(k-x)}{\delta_\pi^2}\right][(k-x)(2+x)2y - y^2(4-x^2) - 2(x^2-4\delta_\pi^2)^{1/2}(y^2-4\delta_i^2)^{1/2} z(xy+k-x) \\
& \qquad + (x^2-4\delta_\pi^2)(y^2-4\delta_i^2)z^2 + 8\delta_i^2(1-\delta_\pi^2)] \\
& \quad + \xi^2(0)\left[1-\frac{\lambda_+(k-x)}{\delta_\pi^2}\right]^2 \{(k-x)(2-x)2y - y^2(2-x)^2 + 2(x^2-4\delta_\pi^2)^{1/2}(y^2-4\delta_i^2)^{1/2} z[k-x-y(2-x)]
\end{aligned}
$$

$$-(x^2-4\delta_\pi^2)(y^2-4\delta_i^2)z^2+8\delta_i^2(k-x)\}\Big](1+F^2)$$

$$-32F\delta_l\delta_i\left[k+x+2\xi(0)\left[1-\frac{\lambda_+(k-x)}{\delta_\pi^2}\right](1-\delta_\pi^2)+\xi^2(0)\left[1-\frac{\lambda_+(k-x)}{\delta_\pi^2}\right]^2(k-x)\right]\Bigg\}, \quad (10)$$

where

$$y=\frac{2E(\nu_i)}{m_K}$$

$$=\frac{2((k+\delta_i^2-\delta_l^2-x)(2-x)\pm(x^2-4\delta_\pi^2)^{1/2}z\{(k+\delta_i^2-\delta_l^2-x)^2-\delta_i^2[(2-x)^2-(x^2-4\delta_\pi^2)z^2]\}^{1/2})}{(2-x)^2-(x^2-4\delta_\pi^2)Z^2}$$

and

$$z=\cos\theta_{\pi\nu_i}\,. \quad (11)$$

Variation of $dW/dx\,dz$ with $z=z_{\pi\nu_e}$, $z_{\pi\nu_\mu}$, and $z_{\pi\nu_\tau}$ in K_{e3}^+ decay, are shown, respectively, in Figs. 11, 12, and 13, with the use of $m(\nu_e)=0$, $m(\nu_\mu)=0.52$ MeV, $m(\nu_\tau)=150$ MeV, and $x=0.6$. In the π-ν_e angular correlation, RHC contributions are distinguishable both for $y_{\min}$ and $y_{\max}$ for $z_{\pi\nu_e}>0.07$, except for $z_{\pi\nu_e}$ in the vicinity of 0.2 for $y_{\max}$ and $z_{\pi\nu_e}>0.08$ for $y_{\min}$. H mixing cannot be distinguished from that of the WM case. Types of mixings are distinguishable except for $z_{\pi\nu_e}>0.8$ for $y_{\min}$. The general features of π-ν_μ and π-ν_τ angular correlations (Figs. 12 and 13) in the K_{e3}^+ decay are identical to those of the π-ν_e correlations. π-ν_e, π-ν_μ, and π-ν_τ angular correlations in the $K_{\mu3}^+$ decay are shown in Figs. 14, 15, and 16, respectively. RHC contributions, in all these correlations, are substantial for both H and KM mixings. Types of mixings are easily distinguishable except in the π-ν_μ angular correlation.

G. π-ν_i energy correlations in K_{l3}^+ decays

The expressions for π-ν_i energy correlations can be obtained from that of π-l energy correlations, Eqs. (8) and (9), by making the replacements $m_l\leftrightarrow m(\nu_i)$, $E_l\rightarrow E(\nu_i)$, $\theta_{\pi l}\rightarrow\theta_{\pi\nu_i}$, and $\sum_{i=1}^3|U_{li}|^2=|U_{li}|^2$:

$$\frac{dW}{dx\,dy}=\frac{C^2|U_{li}|^2G'^2V_{12}^2m_K^5f_+^2(0)}{128\pi^3}\left[1+\frac{\lambda_+(k-x)}{\delta_\pi^2}\right]^2$$

$$\times\Bigg\{(1+F^2)\Big[[(2+x)(1-\delta_\pi^2)+(x^2-4\delta_\pi^2)]2y-y^2(2+x)^2$$

$$+[2(k-x+\delta_i^2-\delta_l^2)-y(2-x)][y(6+x)-2(4+\delta_i^2-\delta_l^2)]+8\delta_i^2(k+x)$$

$$+2\xi(0)\left[1-\frac{\lambda_+(k-x)}{\delta_\pi^2}\right]\{2y(2+x)(k-x)-y^2(4-x^2)$$

$$+[2(k-x+\delta_i^2-\delta_l^2)-y(2-x)](2\delta_i^2-2\delta_l^2-xy-2y)+8\delta_i^2(1-\delta_\pi^2)\}$$

$$+\xi^2(0)\left[1-\frac{\lambda_+(k-x)}{\delta_\pi^2}\right]^2\{(k-x)(2-x)2y$$

$$-y^2(2-x)^2[2(k-x+\delta_i^2-\delta_l^2)-y(2-x)](xy-4y+2\delta_i^2+2\delta_l^2)$$

$$+8\delta_l^2(k-x)\}\Big]$$

$$-4F\delta_l\delta_i\left[k+x+2\xi(0)\left[1-\frac{\lambda_+(k-x)}{\delta_\pi^2}\right](1-\delta_\pi^2)+\xi^2(0)\left[1-\frac{\lambda_+(k-x)}{\delta_\pi^2}\right]^2(k-x)\right]\Bigg\}, \quad (12)$$

with

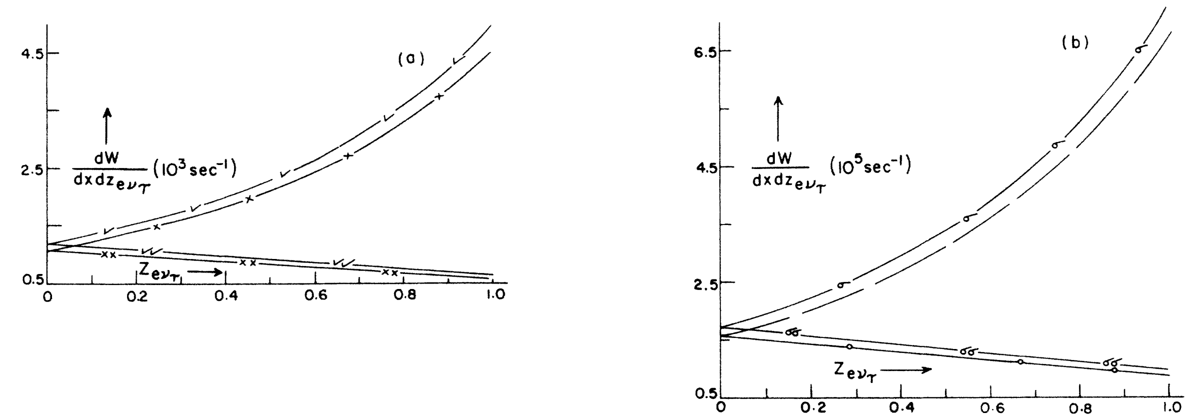

FIG. 25. e-ν_τ angular correlation in K_{e3}^{+} decay with (a) HM and (b) KM the description of the curves is identical to that given in Figs. 24(a) and 23.

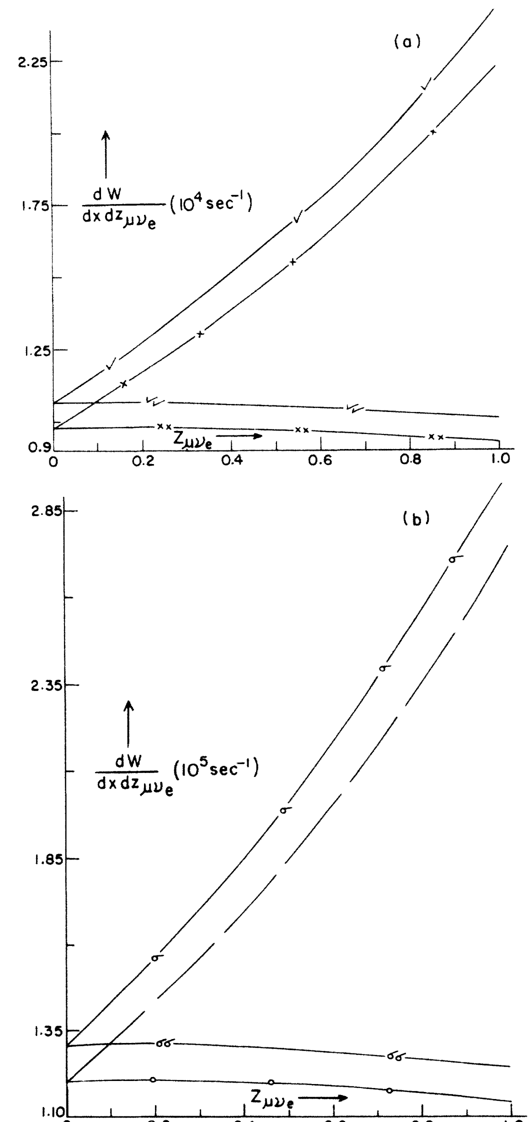

FIG. 26. μ-ν_e angular correlation in $K_{\mu 3}^{+}$ decay with (a) HM and (b) KM the description of the curves is identical to that given in Figs. 24(a) and 23.

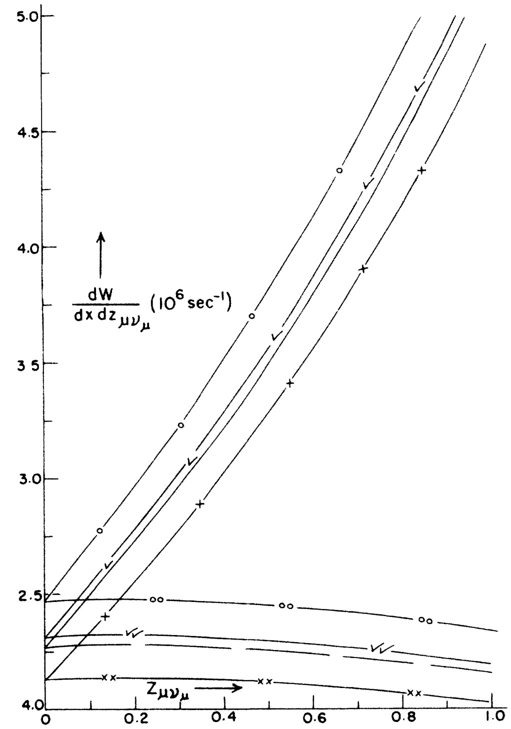

FIG. 27. μ-ν_μ angular correlation in $K_{\mu 3}^{+}$ decay. The solid and one-circle curves are for LHC + WM and LHC + RHC + WM, respectively, with $y_{\max}$. Dashed and two-circle curves are for LHC + WM and LHC + RHC + WM, respectively, with $y_{\min}$. The description of other curves is identical to that given in Fig. 24(a).

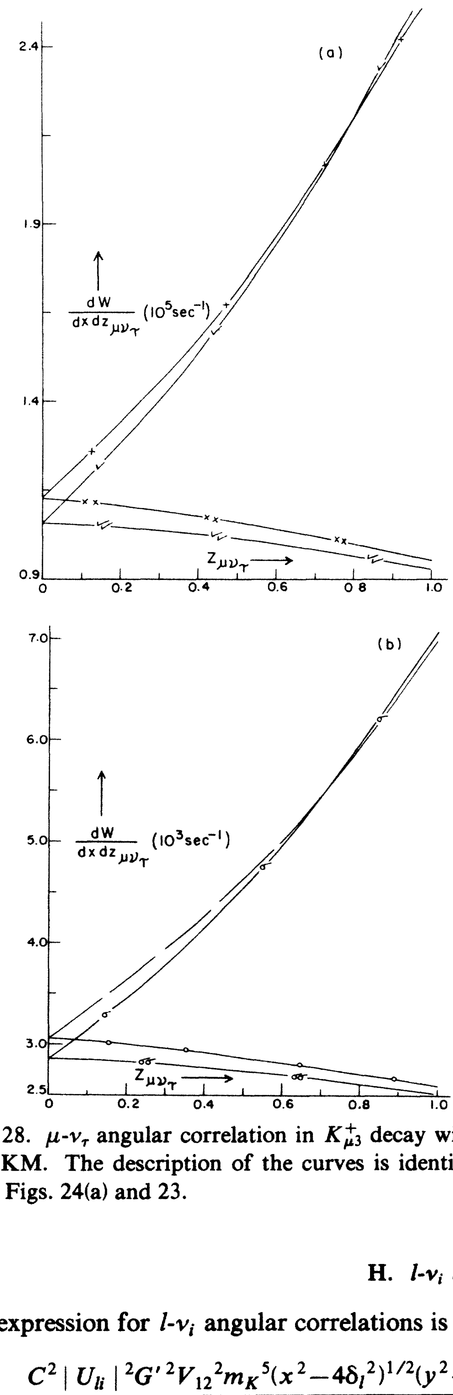

FIG. 28. μ-ν_τ angular correlation in $K_{\mu 3}^+$ decay with (a) HM and (b) KM. The description of the curves is identical to that given in Figs. 24(a) and 23.

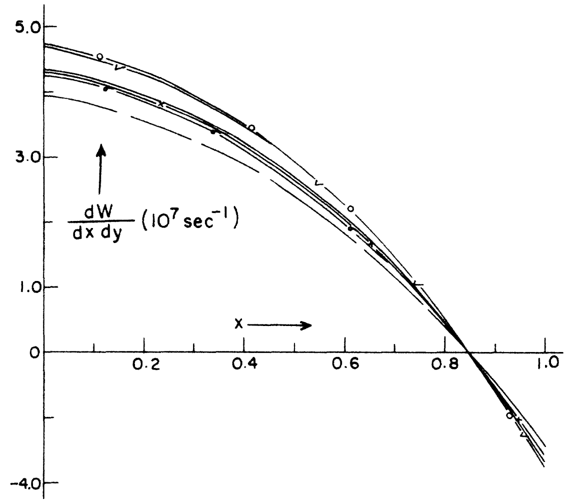

FIG. 29. e-ν_e energy correlation in K_{e3}^+ decay. The description of the curves is identical to that given in Figs. 17 and 18.

$$x=\frac{2E_\pi}{m_K},\quad y=\frac{2E(\nu_i)}{m_K}\ . \tag{13}$$

π-ν_e, π-ν_μ, and π-ν_τ energy correlations, in K_{e3}^+ decay, are shown, respectively, in Figs. 17, 18, and 19, taking $m(\nu_e)=0$, $m(\nu_\mu)=0.52$, $m(\nu_\tau)=150$ MeV, and $y=0.65$. In π-ν_e energy correlation, the RHC contributions are transparent for all values of $x>0.65$, both for WM as well as KM mixing cases. The H mixing part cannot, however, be distinguished from that of WM. H and KM mixings are discernible. The general pattern of π-ν_μ and π-ν_τ energy correlations are identical to that of the π-ν_e energy correlation except for differences in numerical values. RHC contributions are negligible in the π-ν_μ case involving H mixing.

π-ν_e, π-ν_μ, and π-ν_τ energy correlations in the $K_{\mu 3}^+$ decay are shown, respectively, in Figs. 20, 21, and 22. The general patterns are identical to those in the K_{e3}^+ decay.

H. l-ν_i angular correlations in K_{l3}^+ decays

The expression for l-ν_i angular correlations is given by

$$\frac{dW}{dx\,dz}=\frac{C^2\,|\,U_{li}\,|^2 G'^2 V_{12}^2 m_K^5 (x^2-4\delta_l^2)^{1/2}(y^2-4\delta_i^2) f_+^2(0)}{256\pi^3[(2-x)(y^2-4\delta_i^2)^{1/2}+(x^2-4\delta_l^2)^{1/2}yz]}\left[1+\frac{\lambda_+(x+y+\delta_\pi^2-1)}{\delta_\pi^2}\right]^2$$

$$\times\Bigg\{(1+F^2)\Bigg[8(y-\delta_i^2)(x-\delta_l^2)-[xy-z(x^2-4\delta_l^2)^{1/2}(y^2-4\delta_i^2)^{1/2}](4-\delta_l^2-\delta_i^2)$$

$$+2\xi(0)\left[1-\frac{\lambda_+(x+y+\delta_\pi^2-1)}{\delta_\pi^2}\right]\{4\delta_i^2(x-\delta_l^2)+4\delta_l^2(y-\delta_i^2)$$

$$-[xy-z(x^2-4\delta_l^2)^{1/2}(y^2-4\delta_i^2)^{1/2}](\delta_l^2+\delta_i^2)\}$$

$$+\xi^2(0)\left[1-\frac{\lambda_+(x+y+\delta_\pi^2-1)}{\delta_\pi^2}\right]^2\{\,[xy-z(x^2-4\delta_l^2)^{1/2}(y^2-4\delta_i^2)^{1/2}]$$

$$\times(\delta_l^2+\delta_i^2)+8\delta_l^2\delta_i^2\}\Bigg]$$

$$-4F\delta_l\delta_i\left[2(3-x-y+\delta_\pi^2)+4\xi(0)\left[1-\frac{\lambda_+(x+y+\delta_\pi^2-1)}{\delta_\pi^2}\right](1-\delta_\pi^2)\right.$$

$$\left.+\xi^2(0)\left[1-\frac{\lambda_+(x+y+\delta_\pi^2-1)}{\delta_\pi^2}\right]^2[2\delta_i^2+2\delta_l^2+xy-z(x^2-4\delta_l^2)^{1/2}(y^2-4\delta_i^2)^{1/2}]\right]\Bigg\}, \qquad (14)$$

with $x=2E_l/m_K$,

$$y=\frac{2E(\nu_i)}{m_K}$$

$$=\frac{2((1+\delta_l^2+\delta_i^2-\delta_\pi^2-x)(2-x)\pm z(x^2-4\delta_l^2)^{1/2}\{(1+\delta_l^2+\delta_i^2-\delta_\pi^2-x)^2-\delta_i^2[(2-x)^2-(x^2-4\delta_l^2)z^2]\}^{1/2})}{(2-x)^2-(x^2-4\delta_l^2)z^2}, \qquad (15)$$

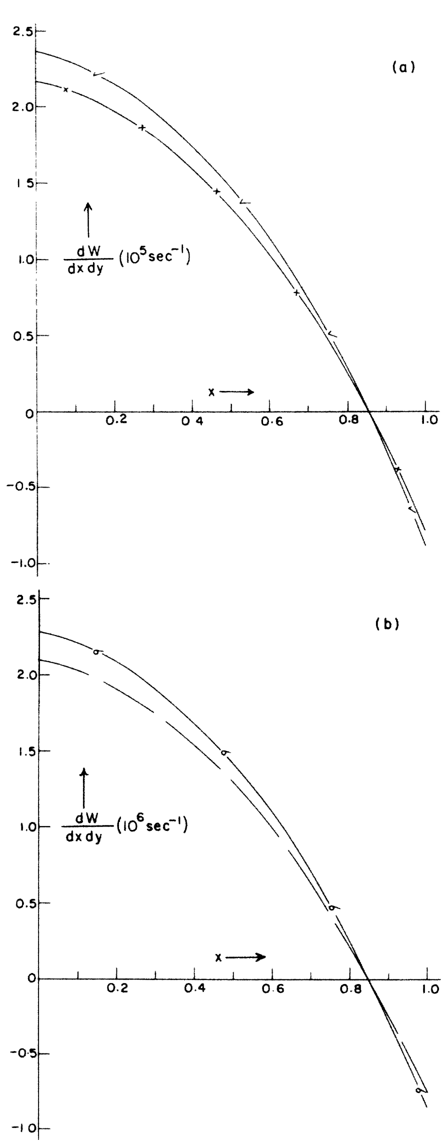

FIG. 30. e-ν_μ energy correlation in K_{e3}^+ decay with (a) HM and (b) KM. The description of the curves is identical to that given in Fig. 18.

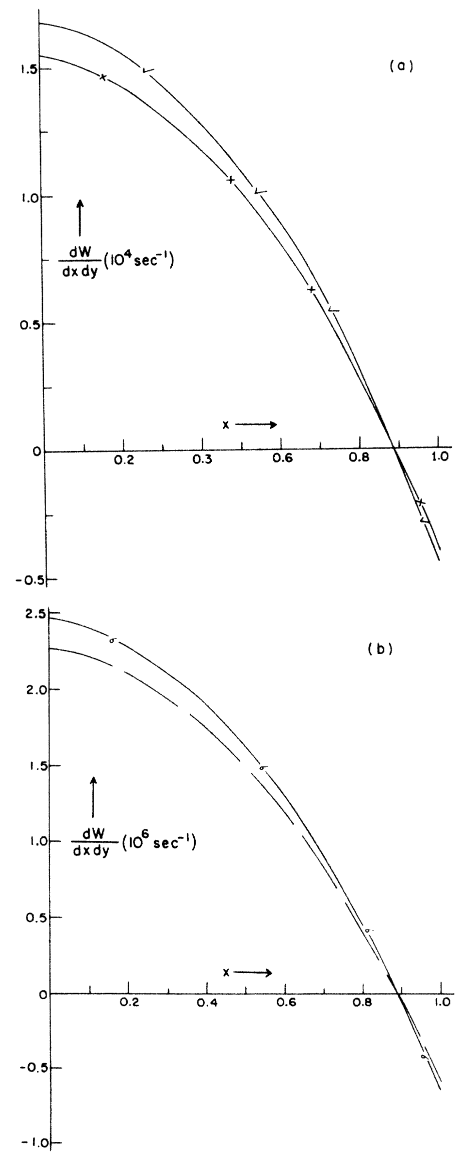

FIG. 31. e-ν_τ energy correlation in K_{e3}^+ decay with (a) HM and (b) KM. The description of the curves is identical to that given in Fig. 18.

and $z=\cos\theta_{l\nu_i}$. e-ν_i angular correlations in K_{e3}^+ decay are shown in Figs. 23—25, taking $m(\nu_e)=0$, $m(\nu_\mu)=0.52$ MeV, $m(\nu_\tau)=150$ MeV, and $x=0.5$. RHC contributions are substantial both for H and KM mixings. Types of mixings are discernible except in e-ν_e angular correlations.

The general features of μ-ν_i angular correlations (Figs. 26—28) are identical to those of e-ν_i in the K_{e3}^+ decay except that the types of mixings are not discernible in μ-ν_μ correlations and RHC contributions are negligible in the μ-ν_τ correlation with $y_{\max}$, for both KM and H mixings in the region $Z_{\mu\nu_\tau}>0.6$.

I. l-ν_i energy correlations in K_{l3}^+ decay

The expression for l-ν_i energy correlations, is given as

$$\begin{aligned}\frac{dW}{dx\,dy}=&\frac{|U_{li}|^2G'^2V_{12}^2C^2m_K{}^5f_+{}^2(0)}{128\pi^3}\left[1+\frac{\lambda_+(x+y+\delta_\pi{}^2-1)}{\delta_\pi{}^2}\right]^2\\
&\times\left\{(1+F^2)\left[4(y-\delta_i{}^2)(x-\delta_l{}^2)-(x+y+\delta_\pi{}^2-1-\delta_l{}^2-\delta_i{}^2)(4-\delta_l{}^2-\delta_i{}^2)\right.\right.\\
&+2\xi(0)\left[1-\frac{\lambda_+(x+y+\delta_\pi{}^2-1)}{\delta_\pi{}^2}\right][2\delta_i{}^2(x-\delta_l{}^2)+2\delta_l{}^2(y-\delta_i{}^2)\\
&-(-\delta_l{}^2+x+y+\delta_\pi{}^2-1-\delta_i{}^2)(\delta_l{}^2+\delta_i{}^2)]\\
&\left.+\xi^2(0)\left[1-\frac{\lambda_+(x+y+\delta_\pi{}^2-1)}{\delta_\pi{}^2}\right]^2[(x+y+\delta_\pi{}^2-1-\delta_l{}^2-\delta_i{}^2)(\delta_l{}^2+\delta_i{}^2)+4\delta_l{}^2\delta_i{}^2]\right]\\
&-4F\delta_l\delta_i\left[3-x-y+\delta_\pi{}^2+2\xi(0)\left[1-\frac{\lambda_+(x+y+\delta_\pi{}^2-1)}{\delta_\pi{}^2}\right](1-\delta_\pi{}^2)\right.\\
&\left.\left.+\xi^2(0)\left[1-\frac{\lambda_+(x+y+\delta_\pi{}^2-1)}{\delta_\pi{}^2}\right]^2(x+y+\delta_\pi{}^2-1)\right]\right\},\end{aligned}\tag{16}$$

with

$$x=\frac{2E_l}{m_K},\quad y=\frac{2E(\nu_i)}{m_K}\,.\tag{17}$$

e-ν_i energy correlations in K_{e3}^+ decay are shown in Figs. 29—31. RHC contributions in e-ν_i correlations are substantial for H and KM mixings in the region $0.75<x<0.9$. In e-ν_μ and e-ν_τ correlations, the RHC contributions are transparent up to $x\simeq0.8$ for both KM and H mixings. Types of mixings are discernible in all cases for $x<0.8$. But H-mixing effects are not distinguishable from the WM case in e-ν_e correlation.

μ-ν_i energy correlations are shown in Figs. 32—34. The general features of μ-ν_i are identical to those of e-ν_i correlations except that types of mixings are not distinct

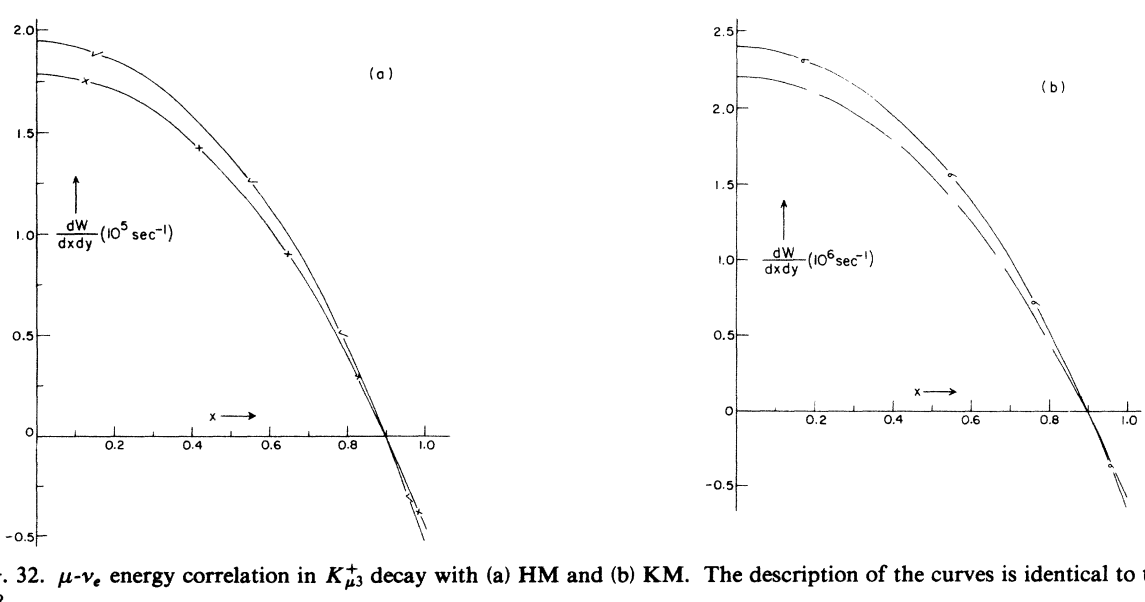

FIG. 32. μ-ν_e energy correlation in $K_{\mu3}^+$ decay with (a) HM and (b) KM. The description of the curves is identical to that given in Fig. 18.

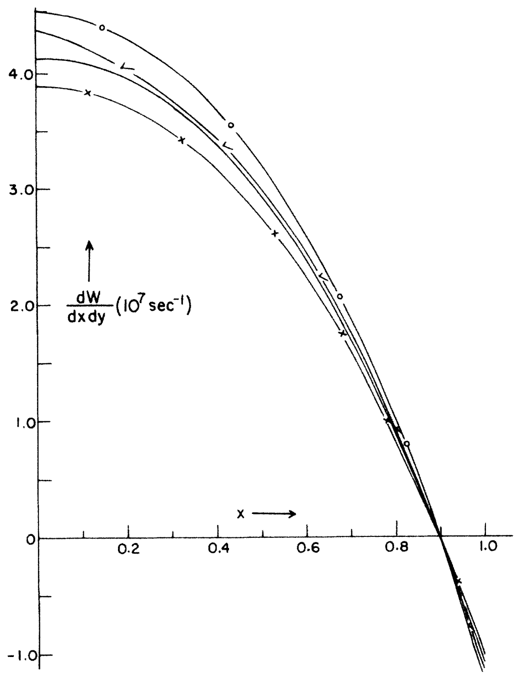

FIG. 33. μ-ν_μ energy correlation in $K_{\mu3}^{+}$ decay. The description of the curves is identical to that given in Figs. 17 and 18. Curves for LHC + KM, LHC + RHC + KM, not shown in the figure, almost coincide with the corresponding curves of WM.

in the μ-ν_μ correlation and RHC contributions in μ-ν_τ correlations are not clear in the vicinity of $x \simeq 0.3$.

J. The ratio $R = W(K_{\mu3}^{+})/W(K_{e3}^{+})$

Using Figs. 3 and 4, we obtain the ratio $R = W(K_{\mu3}^{+})/W(K_{e3}^{+})$, for various values of $m(\nu_3)$, and plot it in Fig. 35. We note that with the use of $F=0.295$, the curve involving contributions from RHC's in the WM case is clearly distinct from that not involving RHC's. The RHC contribution reduces relatively the value of this ratio for all values of $m(\nu_3)$. This conclusion is unambiguous and is suggestive of the fact that this ratio could be an important measure for ascertaining the contributions from RHC's. When mixings (both of H or KM type) are included, RHC contributions cannot be easily discerned.

Using the present experimental value[34] for this ratio $R=0.66\pm0.02$, we calculate $m(\nu_3)$ for various cases which are given in Table II. Variations of this ratio (R) with the RHC factor for some chosen values of $m(\nu_3)$ are shown in Fig. 36, for the purpose of illustration. We emphasize that the experimental value of this ratio can be understood either in terms of finite $m(\nu_3)$ or finite $m(\nu_3)$ plus the RHC, but not in terms of only the RHC contribution. A knowledge of $m(\nu_3)$ may enable us to infer the RHC contribution (or conversely) to obtain a best fit with the experimental value.

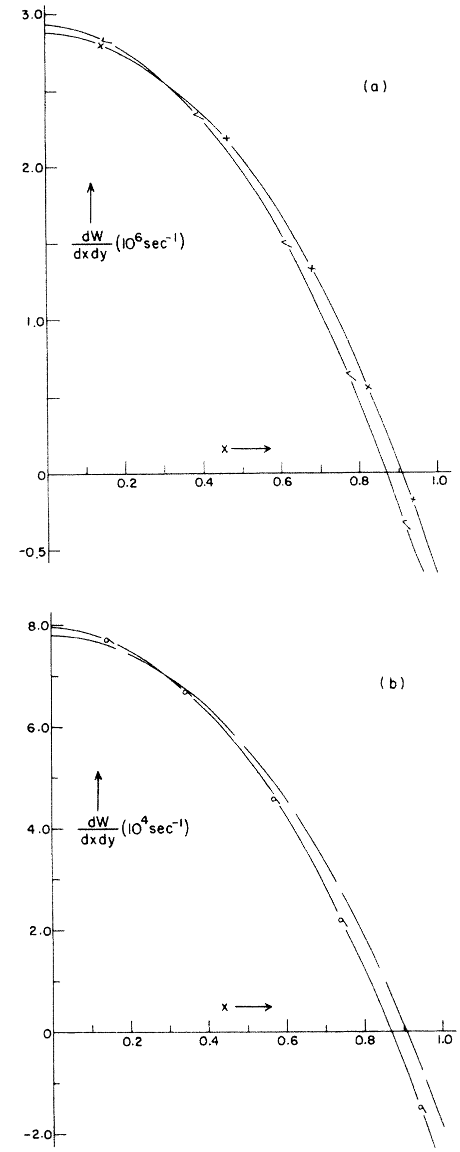

FIG. 34. μ-ν_τ energy correlation in $K_{\mu3}^{+}$ decay with (a) HM and (b) KM. The description of the curves is identical to that given in Fig. 18.

K. Longitudinal lepton polarization in K_{l3}^{+} decays

The longitudinal polarization of the lepton in K_{l3}^{+} decays is given by the expression[37]

$$P_l = \frac{|M(s)|^2 - |M(-s)|^2}{|M(s)|^2 + |M(-s)|^2} = \frac{|M_-|^2}{|M_+|^2} , \tag{18}$$

with $\hat{\mathbf{s}}\cdot\hat{\mathbf{p}}_l = 1$. Expressions for $|M_-|^2$ and $|M_+|^2$, with the inclusion of the RHC, finite neutrino mass, mass mixings, and retention of dominant contribution of δ_3, are given below:

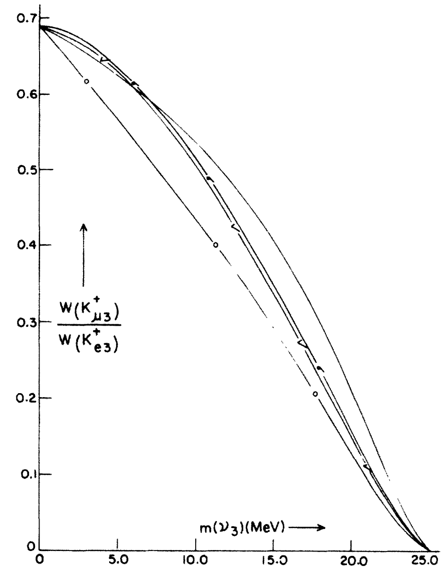

FIG. 35. Variation of ratio $R=W(K^+_{\mu 3})/W(K^+_{e3})$ with $m(\nu_3)$. The solid, one-circle, one-right-mark, and one-σ curves are for LHC + WM, LHC + RHC + WM, LHC + RHC + HM, and LHC + RHC + KM, respectively. Curves for LHC + HM and LHC + KM, not shown in the figure, almost coincide with the curves for LHC + RHC + HM and LHC + RHC + KM, respectively.

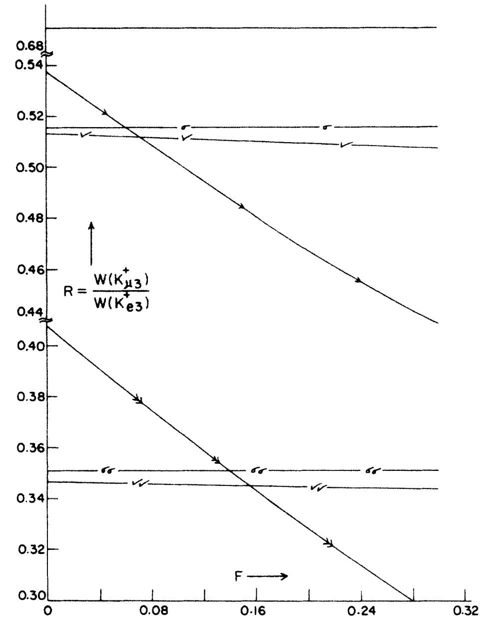

FIG. 36. Variation of ratio $R=W(K^+_{\mu 3})/W(K^+_{e3})$ with the right-handed-current factor F. The solid, one-arrow, and two-arrow curves are for $m(\nu_3)=0$, 100, and 150 MeV with WM. One-right-mark and two-right-mark curves are for $m(\nu_3)=100$ and 150 MeV, respectively, with HM. One- and two-σ curves are for $m(\nu_3)=100$ and 150 MeV, respectively, with KM.

$$
\begin{aligned}
|M_-|^2 = {} & \frac{2G'^2 V_{12}^2 C^2 m_K^4 f_+^2(1-F^2)}{(y^2-4\delta_l^2)^{1/2}} \\
& \times \Bigg\{ (1-U_{l3}^2) \Bigg[(3-\delta_\pi^2+\delta_l^2-x-2y)[2y^2-2\delta_l^2(2+x)-y(1+\delta_\pi^2+\delta_l^2-x)] \\
& \quad -(1+\delta_\pi^2+x)[y(1+\delta_\pi^2+\delta_l^2-x)-2\delta_l^2(2-x)]+2\xi(0)\left[1-\frac{\lambda_+(k-x)}{\delta_\pi^2}\right] \\
& \quad \times \{(y^2-4\delta_l^2)(2-x-y)+(1+\delta_l^2-\delta_\pi^2-y)[2\delta_l^2 x+y(1+\delta_\pi^2+\delta_l^2-x-y)] \\
& \quad -(1-\delta_\pi^2)[y(1+\delta_l^2+\delta_\pi^2-x)-2\delta_l^2(2-x)]\} \\
& \quad -\xi^2(0)\left[1-\frac{\lambda_+(k-x)}{\delta_\pi^2}\right]^2 [y(1+\delta_\pi^2+\delta_l^2-x)-2\delta_l^2(2-x)]\delta_l^2 \Bigg] \\
& + U_{l3}^2 \Big[(3-\delta_\pi^2+\delta_l^2-x-2y-\delta_3^2)[2y^2-2\delta_l^2(2+x)-y(1+\delta_\pi^2+\delta_l^2-\delta_3^2-x)] \\
& \quad -(1+\delta_\pi^2+x)[y(1+\delta_\pi^2+\delta_l^2-\delta_3^2-x)-2\delta_l^2(2-x)] \\
& \quad +2\xi(0)\left[1-\frac{\lambda_+(k-x)}{\delta_\pi^2}\right]\{(y^2-4\delta_l^2)(2-x-y)+(1+\delta_l^2-\delta_\pi^2-\delta_3^2-y)
\end{aligned}
$$

$$\times[2\delta_l^2x+y(1+\delta_\pi^2+\delta_l^2-\delta_3^2-x-y)]$$

$$-(1-\delta_\pi^2)[y(1+\delta_l^2+\delta_\pi^2-\delta_3^2-x)-2\delta_l^2(2-x)]\}$$

$$\times(\delta_3^2-\delta_l^2)\Bigg]\Bigg\}, \tag{19}$$

$$|M_+|^2=2f_+^2G'^2V_{12}^2C^2m_K^4$$

$$\times\Bigg\{(1+F^2)(1-U_{l3}^2)\Bigg[\,3--\delta_\pi^2-x-2y+\delta_l^2)(2+2y-1-\delta_\pi^2-\delta_l^2)-(1+\delta_\pi^2-\delta_l^2-x)(1+\delta_\pi^2+x)$$

$$+\xi(0)\left[1-\frac{\lambda_+(k-x)}{\delta_\pi^2}\right][(1+\delta_\pi^2-\delta_l^2-x)(x+2y-1-\delta_\pi^2-\delta_l^2)$$

$$-2(1+\delta_\pi^2-\delta_l^2-x)(1-\delta_\pi^2)$$

$$+(1+\delta_\pi^2+\delta_l^2-x)(3-\delta_\pi^2+\delta_l^2-x-2y)]$$

$$+\xi^2(0)\left[1-\frac{\lambda_+(k-x)}{\delta_\pi^2}\right]^2[(1+\delta_\pi^2-x-\delta_l^2)(1+\delta_\pi^2+\delta_l^2-x)$$

$$-(1+\delta_\pi^2-\delta_l^2-x)(1+\delta_\pi^2-x)]\Bigg]$$

$$+U_{l3}^2(1+F^2)\Bigg[(3-\delta_\pi^2+\delta_l^2-\delta_3^2-x-2y)(x+2y-1-\delta_\pi^2-\delta_l^2+\delta_3^2)$$

$$-(1+\delta_\pi^2-\delta_l^2-\delta_3^2-x)(1+\delta_\pi^2+x)$$

$$+\xi(0)\left[1-\frac{\lambda_+(k-x)}{\delta_\pi^2}\right][(1+\delta_\pi^2-\delta_l^2+\delta_3^2-x)(x+2y-1-\delta_\pi^2-\delta_l^2+\delta_3^2)$$

$$-2(1+\delta_\pi^2-\delta_l^2-\delta_3^2-x)(1-\delta_\pi^2)$$

$$+(1+\delta_\pi^2+\delta_l^2-\delta_3^2-x)(3-\delta_\pi^2+\delta_l^2-\delta_3^2-x-2y)]$$

$$+\xi^2(0)\left[1-\frac{\lambda_+(k-x)}{\delta_\pi^2}\right]^2[(1+\delta_\pi^2-\delta_l^2+\delta_3^2-x)(1+\delta_\pi^2+\delta_l^2-\delta_3^2-x)$$

$$\times(-\delta_l^2+1+\delta_\pi^2-\delta_3^2-x)(1+\delta_\pi^2-x)]\Bigg]$$

$$-4F\delta_l\delta_3\left[1+\delta_\pi^2+x+2\xi(0)\left[1-\frac{\lambda_+(k-x)}{\delta_\pi^2}\right](1-\delta_\pi^2)+\xi^2(0)\left[1-\frac{\lambda_+(k-x)}{\delta_\pi^2}\right]^2(1+\delta_\pi^2-x)\right]\Bigg\}, \tag{20}$$

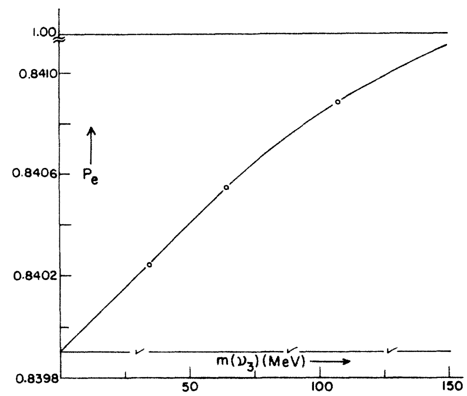

FIG. 37. Variation of electron longitudinal polarization (P_e), in K_{e3}^+ decay, with $m(\nu_3)$. The solid, one-circle, and one-right-mark curves are for LHC + WM, LHC + RHC + WM, and LHC + RHC + HM, respectively. Curves, not shown in the figure, for LHC + HM, LHC + KM, almost coincide with the curve for LHC + WM and the curve for LHC + RHC + KM coincides with the curve for LHC + RHC + HM.

with

$$x=\frac{2E_\pi}{m_K},\ y=\frac{2E_1}{m_K}\ . \tag{21}$$

The expressions for $|M_-|^2$ and $|M_+|^2$ are integrated over x using the limits for x given by Eqs. (5).

The variation of electron longitudinal polarization with $m(\nu_3)$ is shown in Fig. 37. The curve for LHC + RHC for the WM case shows a little variation of P_e with $m(\nu_3)$ for a fixed value of the RHC factor ($F=0.295$). Curves for the LHC and H and KM mixings (not shown in Fig. 37) almost coincide with the curve for the LHC with WM. Also the curves for LHC + RHC with KM (not shown in Fig. 37) almost coincide with the curves for LHC + RHC with H mixing. Thus the types of mixings cannot be distinguished. The curve with LHC

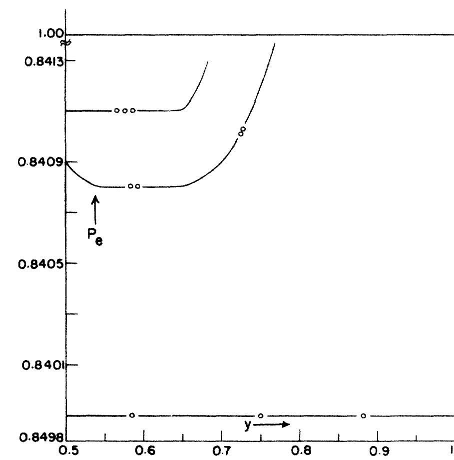

FIG. 39. Variation of electron longitudinal polarization (P_e) with electron energy y. The solid, one-circle, two-circle, and three-circle curves are for $m(\nu_3)=0$ with LHC + WM, $m(\nu_3)=0$ with LHC + RHC + WM, $m(\nu_3)=100$ MeV with LHC + RHC + WM, and $m(\nu_3)=150$ MeV with LHC + RHC + WM, respectively. Curves for $m(\nu_3)=100$ and 150 MeV with LHC + WM, LHC + HM, LHC + KM, and LHC + RHC + HM, LHC + RHC + KM, not shown in the figure, almost coincide with the curve for $m(\nu_3)=0$ with LHC + WM, and LHC + RHC + WM, respectively.

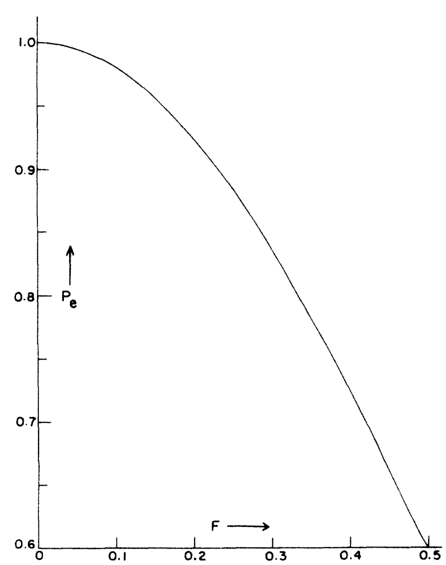

FIG. 38. Variation of electron longitudinal polarization (P_e) with the right-handed-current factor F. The solid curve is for polarization with $m(\nu_3)=0$ and WM. Curves for $m(\nu_3)=100$ and 150 MeV with HM, KM, and WM, not shown in the figure, almost coincide with the solid curve.

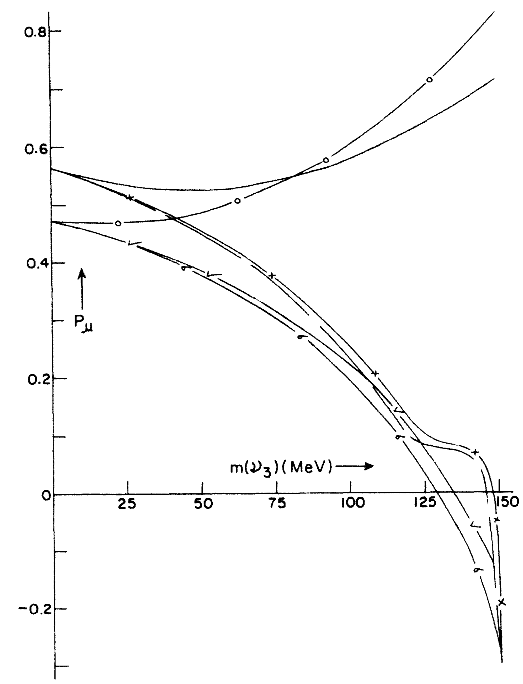

FIG. 40. Variation of muon longitudinal polarization (P_μ) with $m(\nu_3)$. The description of the curves is identical to that given in Fig. 3.

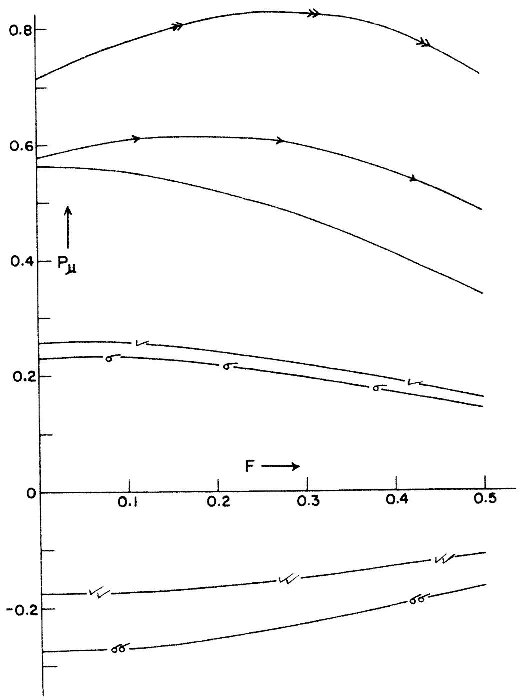

FIG. 41. Variation of muon longitudinal polarization (P_μ) with the right-handed-current factor. The description of the curve is identical to that given in Fig. 36.

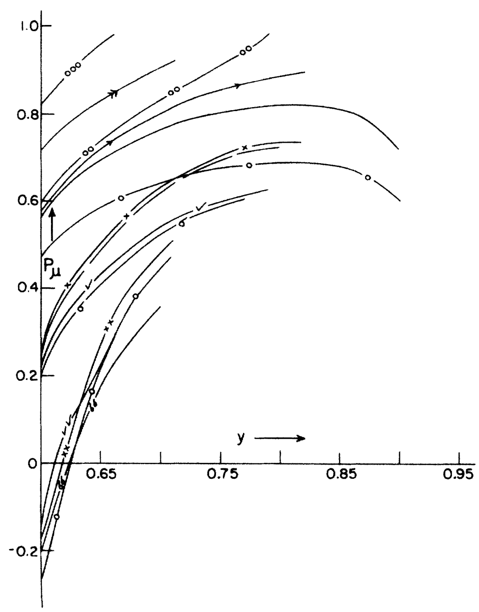

FIG. 42. Variation of muon longitudinal polarization (P_μ) with muon energy y. The dashed curve is for $m(\nu_3)=100$ MeV with LHC + KM. The description of the other curves is identical to that given in Figs. 1 and 2.

+ RHC + WM is, however, distinct from that of LHC + WM, and, does not show any variation with $m(\nu_3)$.

In Fig. 38, variation of P_e with the RHC factor F is shown. It is not possible to distinguish between curves with $m(\nu_3)=0$ from those with finite $m(\nu_3)$, as well as from those involving H and KM mixings. These two results lead us to conclude that a value of P_e smaller than +1 will be indicative of the presence of the RHC contribution. This conclusion is independent of contributions from finite $m(\nu_3)$ as well as H or KM mixings.

Variation of P_e with the electron energy y is shown in Fig. 39. P_e for the case $m(\nu_3)=0$, for the LHC + RHC, WM case shows no variation with y. However, the value P_e is reduced by a constant factor. The curves for LHC + RHC for WM with $m(\nu_3)=100$ and 150 MeV show a little variation of P_e with y, below and beyond a certain value of y. The mixing effects are, however, not discernible for various cases. Thus an indication of variation of P_e with y could be suggestive of the contribution from a finite neutrino mass. This, of course, would require a highly sensitive measurement of P_e vs y.

The variations of muon polarization with $m(\nu_3)$ are shown in Fig. 40 for $y=0.6$. The curve for LHC + RHC + WM is distinct from that for LHC + WM except around $m(\nu_3)=85$ MeV. The types of mixings are difficult to distinguish. However, the behavior of these curves, namely, the curves pertaining to LHC + RHC with H or KM mixings are distinct from those of LHC + HM or LHC + KM over almost the entire range of variation excepting at the tail end. The variations of P_μ with the RHC factor F are shown in Fig. 41 for various cases.

In Fig. 42, variation of P_μ with the muon energy (y) for various cases is shown. The curve LHC + RHC + WM with $m(\nu_3)=0$ is clearly distinguishable from the LHC + WM with $m(\nu_3)=0$ for all values of y; the RHC contribution decreases the values of P_μ relatively. When finite $m(\nu_3)=100$ and 150 MeV are included, the polarization curves involving the RHC lie above the corresponding curves not involving the RHC. Thus the RHC factor enhances the values of P_μ for all values of y.

When mixing is included (whether H or KM), the curves inclusive of the RHC factor lie below the corresponding curves not involving the RHC factor for $m(\nu_3)=100$ and 150 MeV for $y>0.64$. These values of $m(\nu_3)$ are chosen only for illustration purposes. Thus a study of variation of P_μ with y could be a useful place to ascertain the RHC contribution, finite $m(\nu_3)$ as well as mixings.

III. SUMMARY AND CONCLUSIONS

(1) RHC contributions are transparent in the following parameters: pion energy spectrum in both K^+_{e3} as well as $K^+_{\mu 3}$ decays, when no mixing is involved [for finite $m(\nu_3)=100$ and 150 MeV, these contributions are distinct except at the tail end of the spectrum]; decay probability; π-l angular and energy correlations; lepton energy spectrum; π-ν_i angular and energy correlations; l-ν_i energy and angular correlations; in the ratio R involving no mixing; and in electron and muon longitudinal polarizations.

(2) Finite-neutrino-mass $m(\nu_3)$ effects are distinct in the following parameters: pion energy spectrum in both K^+_{e3} and $K^+_{\mu 3}$ decays involving no mixing; decay probabili-

ty; π-l angular and energy correlations; lepton energy spectrum; the ratio R; and the muon longitudinal polarizations.

(3) Mixing effects could possibly be seen in decay probabilities of K_{e3}^{+} and $K_{\mu 3}^{+}$ decays, lepton energy spectrum in the range $0.5<y<0.7$, the existence of energy and angular correlations π-ν_μ, π-ν_τ, e-ν_μ, e-ν_τ in K_{e3}^{+} decay and π-ν_e, π-ν_τ, μ-ν_e, μ-ν_τ in $K_{\mu 3}^{+}$ decay, the variation of ratio R with $m(\nu_3)$ for $m(\nu_3)>80$ MeV, and in the variation of muon longitudinal polarization against muon energy y.

(4) The types of mixings in the lepton sector are difficult to discern. However, it may possibly be done in the following: lepton energy spectrum in the range $0.5<y<0.7$; all π-ν_i angular and energy correlations except in π-ν_μ in the $K_{\mu 3}^{+}$ decay; and in the variation of muon longitudinal polarization with y.

(5) Contributions from RHC's may be distinguished from those of a finite neutrino mass $m(\nu_3)$ in the following: (i) pion energy spectrum curves, lying above that for $m(\nu_3)=0$, are explainable only in terms of RHC contributions, whereas those involving a finite $m(\nu_3)$ with or without RHC lie below this curve. (ii) Decay probability—RHC contributions enhance the decay probabilities whereas a finite $m(\nu_3)$ reduces it. (iii) π-l angular and energy correlations—the behavior has the features described in (i). (iv) Lepton energy spectrum—the variation of dW/dy in the range $0.5<y<0.7$. (v) The ratio R for the without-mixing case. (vi) Variation of electron and muon longitudinal polarizations with y.

(6) A few notable conclusions follow.

(i) The presently known decay probabilities of K_{e3}^{+} and $K_{\mu 3}^{+}$ decays can be explained either with the inclusion of a RHC contribution or a finite $m(\nu_3)+$RHC contribution, but not in terms of a finite neutrino mass $m(\nu_3)$ only.

(ii) The value of the ratio R (0.66 ± 0.02) can be explained either with the inclusion of a finite neutrino mass $m(\nu_3)$ or a finite $m(\nu_3)+$RHC contribution, but not in terms of a RHC contribution only.

(iii) The existence of electron polarization $P_e<+1$ will be indicative of a finite RHC contribution independent of $m(\nu_3)$. A departure of P_e from the constant value for any value (s) of y will be indicative of the contribution of finite $m(\nu_3)$. Such unambiguous conclusions for muon polarization[38] P_μ are, however, not possible in which RHC contributions as well as those from a finite $m(\nu_3)$ are not distinct.

(7) The range of values of $m(\nu_3)$ calculated using presently known parameters with the inclusion of the RHC contribution lie between (14 ± 8)–(44 ± 5) MeV and are consistent with the presently known limits.[20]

(8) The calculated limits on the RHC factor F, neglecting the neutrino mass, are <0.26 and <0.22 for K_{e3}^{+} and $K_{\mu 3}^{+}$ decays, respectively, which are consistent with the presently known limit.[17]

ACKNOWLEDGMENTS

The authors wish to express their thanks to Professor S. Lokanathan for fruitful discussions. They are also thankful to Dr. Y. Vijay for assistance in computation work. R.R.L.S. is grateful to the University Grants Commission, India for providing him with financial support at the Physics Department, University of Rajasthan, Jaipur, India.

---

*On academic leave from Government College, Dholpur, Rajasthan, India.

[1]S. L. Glashow, Nucl. Phys. **B22**, 579 (1961); A. Salam, in *Elementary Particle Theory: Relativistic Groups and Analyticity (Nobel Symposium No. 8)*, edited by N. Svartholm (Almqvist and Wiksell, Stockholm, 1968), p. 367; S. Weinberg, Phys. Rev. Lett. **19**, 1264 (1967).

[2]UA1 Collaboration, G. Arnison *et al.*, Phys. Lett. **112B**, 103 (1983); **126B**, 398 (1983); UA2 Collaboration, M. Banner *et al.*, *ibid.* **122B**, 476 (1983); P. Bagnaia *et al.*, *ibid.* **129B**, 130 (1983); C. Rubbia, in *Proceedings of the International European Physical Society Conference on High Energy Physics, Brighton, 1983*, edited by J. Guy and C. Costain (Rutherford Appleton Laboratory, Chilton, Didcot, Oxfordshire, England, 1983).

[3]See, for example, D. V. Nanopoulos, in *Proceedings of the XXII International Conference on High Energy Physics, Leipzig, 1984*, edited by A. Meyer and E. Wieczorek (Academie der Wissenschaften der DDR, Zeuthen, DDR, 1984).

[4]J. C. Pati and A. Salam, Phys. Rev. D **10**, 275 (1974); G. Senjanović and R. N. Mohapatra, *ibid.* **12**, 1502 (1975).

[5]G. Senjanović and R. N. Mohapatra, Phys. Rev. D **23**, 165 (1981).

[6]R. N. Mohapatra and J. C. Pati, Phys. Rev. D **11**, 566 (1975); D. Chang, Nucl. Phys. **B214**, 435 (1983).

[7]H. Georgi, in *Particles and Fields—1974*, proceedings of the Meeting of the APS Division of Particles and Fields, Williamsburg, Virginia, edited by C. E. Carlson (AIP, New York, 1975); H. Fritzsch and P. Minkowski, Ann. Phys. (N.Y.) **93**, 193 (1975).

[8]For reviews of left-right symmetry, see G. Senjanović, Nucl. Phys. **B153**, 334 (1979); R. N. Mohapatra, lectures at NATO Summer School on Particle Physics, Munich, 1983 (unpublished).

[9]M. A. Beg, R. V. Budny, R. N. Mohapatra, and A. Sirlin, Phys. Rev. Lett. **38**, 1252 (1977).

[10]G. Beall and Myron Bander, Phys. Rev. Lett. **48**, 848 (1981).

[11]T. Oka, Phys. Rev. Lett. **50**, 1423 (1983).

[12]Wai-Yee Keung and G. Senjanović, Phys. Rev. Lett. **50**, 1427 (1983).

[13]E. Masso, Phys. Rev. Lett. **52**, 1956 (1984).

[14]P. Herczeg, Phys. Rev. D **28**, 200 (1983); P. Herczeg and T. Oka, *ibid.* **20**, 475 (1984); P. Herczeg and C. M. Hoffman, *ibid.* **29**, 1954 (1984).

[15]A. Garcia, Phys. Rev. D **3**, 2638 (1971).

[16]J. Carr *et al.*, Phys. Rev. Lett. **51**, 627 (1983).

[17]R. S. Hayano *et al.*, Phys. Rev. Lett. **52**, 329 (1984).

[18]S. Boris *et al.* (unpublished), quoted by V. A. Lubimov, in *Proceedings of the International Europhysics Conference on High Energy Physics, Brighton, 1983* (Ref. 2). See also V. A. Lubimov *et al.*, Phys. Lett. **94B**, 266 (1980).

[19]D. C. Lu *et al.*, Phys. Rev. Lett. **45**, 1066 (1980); M. Duam *et al.*, Phys. Rev. D **20**, 2692 (1979); M. LeCoultre *et al.*, in *Massive Neutrinos in Astrophysics and Particle Physics*, proceedings of the Moriond Workshop, La Plagne, France, 1984, edited by J. Tran Thanh Van (Editions Frontières, Gif-

sur-Yvette, 1984).

[20]C. Matteuzzi *et al.*, Phys. Rev. Lett. **52**, 1869 (1984); Phys. Rev. D **32**, 800 (1985); G. B. Mills *et al.*, Phys. Rev. Lett. **54**, 624 (1985).

[21]R. R. L. Sharma and N. K. Sharma, Pramana **21**, 329 (1983).

[22]R. R. L. Sharma and N. K. Sharma, Phys. Rev. D **29**, 1533 (1984); **30**, 2418 (1984); J. Babson and Ernest Ma, Z. Phys. C **20**, 5 (1983); Phys. Rev. D **26**, 2497 (1982).

[23]R. E. Shrock, Phys. Lett. **96B**, 159 (1980).

[24]R. E. Shrock, Phys. Rev. D **24**, 1232 (1981); **24**, 1275 (1981).

[25]J. F. Cavaignac *et al.*, Laboratoire d'Annecy-Le-Vieux de Physique des Particules, France Report No. Exp. 84-03 (unpublished); Institut des Sciences Nucléaires de Grenoble, France Report No. 84-11, 1984 (unpublished).

[26]F. Bergsma *et al.*, CERN-Hamburg-Amsterdam-Rome-Moscow (CHARM) Collaboration, Phys. Lett. **128B**, 361 (1983).

[27]V. Barger, K. Whisnant, and R. J. N. Phillips, Phys. Rev. D **22**, 1636 (1980).

[28]D. Silverman and A. Soni, Phys. Rev. D **27**, 58 (1983).

[29]R. R. L. Sharma and N. K. Sharma, Phys. Rev. D **31**, 2251 (1985).

[30]P. H. Frampton and P. Vogel, Phys. Rep. **82**, 339-388 (1982); S. M. Bilenky and B. Pontecorvo, Phys. Rep. **41**, 225 (1978).

[31]H. Leutwyler and M. Roos, Z. Phys. C **25**, 91 (1984).

[32]M. Kobayashi and K. Maskawa, Prog. Theor. Phys. **49**, 652 (1973).

[33]R. E. Shrock and L. L. Wang, Phys. Rev. Lett. **41**, 1692 (1978); M. Bourquin *et al.*, Z. Phys. C **21**, 27 (1983).

[34]Particle Data Group, Rev. Mod. Phys. **56**, S102 (1984).

[35]L. M. Chounet, J. M. Gaillard, and M. K. Gallard, Phys. Rep. **4C**, 199 (1972).

[36]P. Kalyniak and John N. Ng, Phys. Rev. D **24**, 1874 (1981).

[37]*Advances in Particle Physics*, edited by R. L. Cool and R. E. Marshak (Interscience, New York, 1968), Vol. 1, pp. 462–466.

[38]D. Cutts, T. Elioff, and R. Stiening, Phys. Rev. **138**, B969 (1965).